JBC RESEARCH ARTICLE

Mapping of the fibrinogen-binding site on the staphylocoagulase C-terminal repeat region

Received for publication, December 3, 2021 Published, Papers in Press, December 13, 2021,
https://doi.org/10.1016/j.jbc.2021.101493

Ashoka A. Maddur[1,*], Markus Voehler[2], Peter Panizzi[3], Jens Meiler[4,5], Paul E. Bock[6,†], and Ingrid M. Verhamme[6,*]

From the [1]FUJIFILM Diosynth Biotechnologies, College Station, Texas, USA; [2]Vanderbilt Center for Structural Biology, Vanderbilt University, Nashville, Tennessee, USA; [3]Department of Drug Discovery and Development, Harrison School of Pharmacy, Auburn University, Auburn, Alabama, USA; [4]Department of Chemistry, Vanderbilt University, Nashville, Tennessee, USA; [5]Institute for Drug Discovery, Leipzig University Medical School, Leipzig, Germany; [6]Department of Pathology, Microbiology, and Immunology, Vanderbilt University Medical Center, Nashville, Tennessee, USA

Edited by Wolfgang Peti

Fibrin (Fbn) deposits are a hallmark of staphylocoagulase (SC)-positive endocarditis. Binding of the N terminus of *Staphylococcus aureus* SC to host prothrombin triggers formation of an active SC·prothrombin* complex that cleaves host fibrinogen to Fbn. In addition, the C-terminal domain of the prototypical SC contains one pseudorepeat (PR) and seven repeats (R1 → R7) that bind fibrinogen/Fbn fragment D (frag D) by a mechanism that is unclear. Here, we define affinities and stoichiometries of frag D binding to C-terminal SC constructs, using fluorescence equilibrium binding, NMR titration, alanine scanning, and native PAGE. We found that constructs containing the PR and single repeats bound frag D with K_D ∼50 to 130 nM and a 1:1 stoichiometry, indicating a conserved binding site bridging the PR and each repeat. NMR titration of PR–R7 with frag D revealed that residues 22 to 49, bridging PR and R7, constituted the minimal peptide (MP) for binding, corroborated by alanine scanning, and binding of labeled MP to frag D. MP alignment with the PR–R and inter-repeat junctions identified critical conserved residues. Full-length PR–(R1 → R7) bound frag D with K_D ∼20 nM and a stoichiometry of 1:5, whereas constructs containing the PR and various three repeats competed with PR–(R1 → R7) for frag D binding, with a 1:3 stoichiometry. These findings are consistent with binding at PR–R and R–R junctions with modest inter-repeat sequence variability. CD of PR–R7 and PR–(R1 → R7) suggested a disordered flexible structure, allowing binding of multiple fibrin(ogen) molecules. Taken together, these results provide insights into pathogen localization on host fibrin networks.

Staphylococcus aureus (*S. aureus*) is the leading cause of hospital-acquired infections targeting the skin, soft tissue, bone, and heart valves. *S. aureus* can cause endocarditis, osteomyelitis, and septicemia (1). Invasive methicillin-resistant infections are responsible for ∼20,000 deaths annually (2). The *S. aureus* staphylocoagulases (SCs) are secreted virulence factors, originally grouped into 12 serotypes based on their genetic diversity (3), and with recent serotype additions now a total of 15 (4, 5). SC contributes to abscess formation, typical of *S. aureus* infection (6–8). Interaction of host fibrinogen (Fbg) with the *S. aureus* virulence factors, clumping factor A and B, FbnA, efb, and SC, was reported previously (9–13); however, several mechanisms underlying these specific Fbg interactions are not yet defined at the molecular level. Coagulase-positive *S. aureus* adheres to exposed subendothelium on heart valves damaged by turbulent blood flow, where deposition of platelets and fibrin (Fbn) creates adhesion foci for circulating bacteria (1). Fbg also facilitates interactions between *S. aureus* and platelets (14). Our previous fluorescence equilibrium binding and native PAGE studies revealed for the first time that Fbg and Fbn bind free SC as well as its complex with host prothrombin (ProT); and that the fragment D (frag D) domain of Fbg/Fbn harbors major interaction sites for binding to the C-terminal repeat region of SC (15, 16). The current work identifies the binding motifs in the C-terminal SC region, essential for interaction with frag D, and defines the stoichiometry of frag D binding to free and ProT-complexed SC.

SC is a bifunctional protein that uses its N terminus for conformational activation of ProT, the precursor of the central clotting protease, thrombin (T). Classical serine proteinase activation requires proteolytic cleavage of the Arg^{15}–Ile^{16} peptide bond in the zymogen (chymotrypsinogen numbering), with release of a new N terminus that inserts in the Ile^{16}-binding pocket to trigger formation of the active site (17, 18). In contrast, our structure–function studies showed that formation of the active site in ProT by SC is a non-proteolytic mechanism, in which SC inserts its N terminus into the zymogen activation pocket, thereby forming a critical salt bridge required for conformational expression of the active site in ProT (19, 20). In the absence of SC, Fbg binds to T at exosite I and is cleaved as a substrate. In the SC·ProT* (* denotes a fully expressed active site) and SC·T complexes, (pro)exosite I is occupied by the tight-binding N-terminal D2 domain, and a new binding site is expressed on these complexes for Fbg as a substrate (21). The SC(1–325) fragment,

† Deceased.

* For correspondence: Ingrid M. Verhamme, ingrid.verhamme@vanderbilt.edu; Ashoka A. Maddur, ashoka.maddur@fujifilm.com.

containing the D1 and D2 domains, is sufficient for expression of this novel Fbg-binding site on the SC·ProT* and SC·T complexes and triggering of proteolytic Fbg cleavage to form Fbn clots.

In addition to the N-terminal D1 and D2 ProT-binding domains, the prototypical full-length SC(1–660) from the *S. aureus* strain Newman D2 Tager 104 also contains a central region with unknown function and a C-terminal domain consisting of one 32-residue pseudorepeat (PR) and seven 27-residue tandem repeats, R1 → R7 (Fig. 1) with highly conserved inter-repeat sequences. Our studies use the Tager 104 sequence with GenBank accession number AY225090.2 as identified by us (19). SC from other strains contains the PR and four to nine repeats (Fig. S1) (22, 23). Fbg binding to SC was recognized previously (14, 24, 25), and we narrowed down this interaction to Fbg frag D binding to the C-terminal domain (15, 16, 26, 27). Binding of Fbg and frag D to the SC C-terminal domain has been studied by turbidity assays, ELISA, isothermal titration calorimetry, and solid-phase Fbg binding of an SC C-terminal domain construct (25, 28, 29). The present work identifies a conserved minimal peptide (MP), required for binding of PR–R constructs to frag D, by equilibrium binding, NMR titration, and alanine (Ala) scanning. The MP sequence bridges the PR and R junctions, exhibits alignment with inter-repeat junctions, and contains a set of conserved residues that are critical for frag D binding. Knowledge of this minimal binding site is useful for future development of mechanism-based antibody drugs targeting the SC C-terminal domain.

We present an in-depth analysis of the potential of SC to bind multiple frag D units at its C-terminal repeat domain, independent of substrate Fbg binding to the catalytic SC·ProT* complex. We show that the full-length C-terminal repeat construct, PR–(R1 → R7) binds frag D with a stoichiometry of ∼5 frag D per construct; and constructs containing a leading PR and three R units in consecutive or arbitrary order bind frag D with a stoichiometry of ∼3. Shortening of the full-length repeat construct or changing the order of repeats did not alter the ability of repeats to bind frag D, reaffirming the requirement of aligned conserved residues at the repeat junctions for formation of multiple binding sites. Consistent with these observations, our data of *in vivo* localization of SC·ProT* complexes to areas rich in Fbg show involvement of a template mechanism that utilizes the SC C-terminal domain (15). The high affinity of multiple binding sites for Fbg/Fbn D domains on a single SC molecule contributes to a mechanism of selective anchoring of proteolytically active SC·ProT* complexes on host Fbn–bacteria vegetations subjected to arterial shear stress.

Results

Sequence alignment of the SC C-terminal repeats

The C-terminal repeat alignment of SC(1–660) *S. aureus* Newman D2 Tager 104 was performed using an online box shade alignment program, http://embnet.vital-it.ch/software/BOX_form.html. Figure 2 shows the sequence alignment of PR, 32 amino acid residues, with R1 to R7, each 27 residues in length. PR and the repeats show a 30 to 40% conserved sequence, and there is >80% pairwise identity among the repeats. Repeats R2, R4, and R5 are identical. We identified the MP sequence as described later, and in Figures 3–11, the MP alignment is shown with the bridging sequences between repeats and conserved residues (*red*) at positions G^{37}, Y^{41}, A^{43}, R^{44}, P^{45}, K^{49}, and P^{50} (PR–R7 numbering). The residues G^{28} and I^{31} are present only in the PR and are replaced with similar size hydrophobic residues A and V in the repeats. PR–Rx constructs used in this study were created with a 10-residue SC sequence preceding the PR to preserve the integrity of a putative binding site; five residues of the SC sequence were added at the

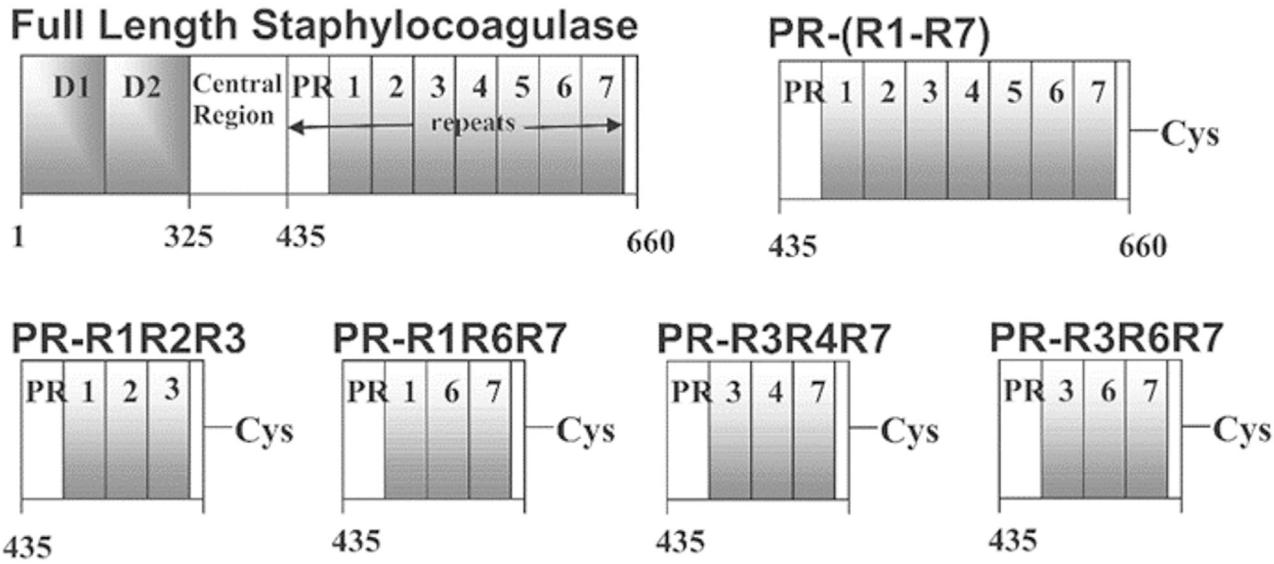

Figure 1. Domain organization of full-length SC and multirepeat constructs. Full-length SC secreted by the *Staphylococcus aureus* Newman D2 Tager 104 contains three major regions: the N-terminal D1 and D2 domains (I), a central region (II), and the C-terminal repeat region (III), consisting of one pseudorepeat (PR) and seven repeats (R1–R7). The five residues at the C-terminal end are conserved (IV). SC, staphylocoagulase.

```
PR   ARPQFNKTPKYVKYRDAGTGIREYNDGTFGYE
R1   ARPRFNKPSETNAYNVTTHANGQVSYG-----
R2   ARPTQNKPSKTNAYNVTTHGNGQVSYG-----
R3   ARPTYKKPSKTNAYNVTTHANGQVSYG-----
R4   ARPTQNKPSKTNAYNVTTHGNGQVSYG-----
R5   ARPTQNKPSKTNAYNVTTHGNGQVSYG-----
R6   ARPTQNKPSKTNAYNVTTHANGQVSYG-----
R7   ARPTYKKPSETNAYNVTTHADGTATYG-----
```

Figure 2. Sequence alignment of the C-terminal pseudorepeat (PR) and the repeats (R1–R7) from SC of *Staphylococcus aureus* Newman D2 Tager 104. The PR contains 32 residues, and the repeats R1–R7 are 27 residues in length. Conserved residues are in *red*. SC, staphylocoagulase.

C-terminal end of constructs ending in R7 to simplify expression, and a Cys residue was introduced for labeling purposes, as detailed in the "Experimental procedures" section.

Size-exclusion chromatography and light scattering

SC(1–325) containing only the N-terminal domains D1 and D2, and full-length SC(1–660) that includes the C-terminal repeats, were chromatographed separately and in mixtures with frag D. Figure 3*A* shows the elution profile of SC(1–325) (*black*), frag D (*red*), and their mixture (*blue*). Light scattering indicated that SC(1–325) (*M*r = 38,000 Da) eluted with an apparent molecular mass of ∼32,500 Da. Frag D (relative molecular mass [M_r], 88,000 Da) showed a hydrodynamic property–related anomaly, eluting in the same apparent molecular mass range, in part because of interaction of frag D with the column matrix. The SC(1–325) and frag D mixture eluted at a position similar to SC(1–325) and frag D alone, suggesting that SC(1–325) does not form a high M_r complex with frag D. Figure 3*B* shows the elution profile of SC(1–660) (*black*), frag D (*red*), and their mixture (*blue*). Light scattering indicated that SC(1–660) (M_r, 74,390 Da) eluted with apparent molecular mass of ∼81,200 Da. The mixture of SC(1–660) and frag D showed a new peak eluting at ∼165,000 Da, suggesting that the C-terminal region of SC(1–660) binds frag D.

Native PAGE of frag D binding to SC(1–660), [5F]PR–R1, the SC(1–660)·[5F]ProT complex, and labeled C-terminal repeat constructs

Formation of multimeric SC(1–660)·frag D complexes was confirmed by native PAGE (Fig. 3*C*). Frag D (lane 10, M_r, 88 KDa) runs faster than SC(1–660) (lane 1, M_r, 74.4 KDa) because of combined differences in isoelectric point, hydrodynamic properties, secondary structure, and native charge density, unlike in SDS-PAGE. Minor frag D proteolysis bands were due to Fbg digestion by trypsin during frag D preparation. Upon binding of frag D to SC(1–660), the SC(1–660)·frag D complex band shifted, starting at twofold molar excess frag D, and the shift and band intensity became more pronounced at increasing frag D (lanes 2–9). Unbound frag D was observed starting at sevenfold molar excess (lanes 7–9), suggesting that the C-terminal region of SC(1–660) binds multiple molecules of frag D, possibly five to six.

Frag D also formed a complex with PR–R1, labeled with 5-iodoacetamidofluorescein (5-IAF) at an engineered C-terminal Cys residue (5-fluorescein [5F]PR–R1) but not with labeled R1 peptide ([5F]R1) or PR ([5F]PR) (Fig. S2).

Tight-binding complexes of SC(1–660) with ProT, covalently labeled at the active site with ([5F]ProT) (30), recruited

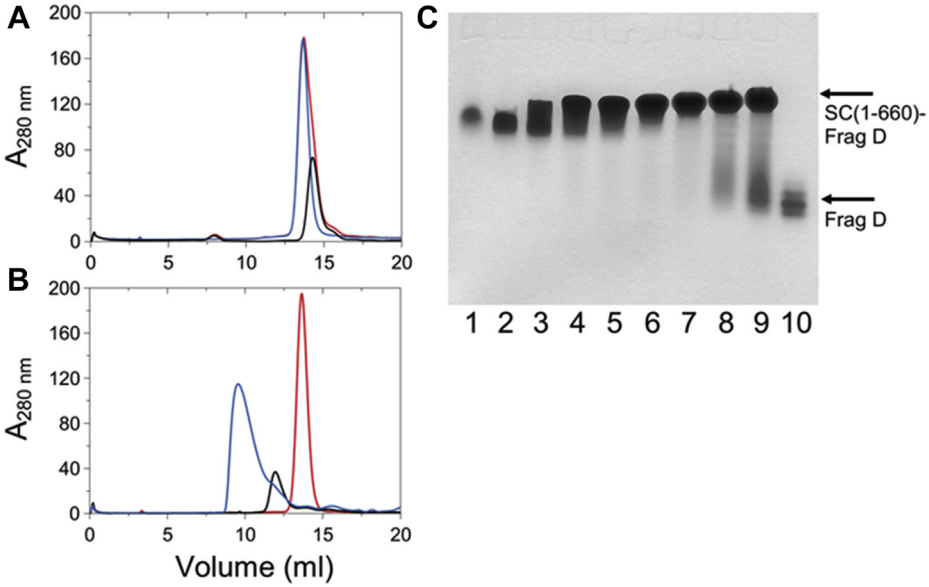

Figure 3. Size-exclusion chromatography of SC(1–325), SC(1–660), and their mixtures with frag D, and native PAGE of SC(1–660) binding to frag D. *A,* elution profiles (absorbance at 280 nm in mOD) of SC(1–325) alone, *black*; frag D alone, *red*; and mixture of SC(1–325) and frag D, *blue. B,* elution profiles of SC(1–660) alone, *black*; frag D alone, *red*; and mixture of SC(1–660) and frag D, *blue*. SC(1–660) forms a high molecular weight complex with frag D as shown by the appearance of new high molecular weight peak. *C,* Coomassie-stained native 6% Tris–glycine PAGE, showing the formation of SC(1–660)·frag D complex. SC(1–660) (4.0 μM) was reacted with frag D (lanes 2–9, at respectively, 4.1, 8.2, 16.4, 20.0, 24.6, 28.6, 32.7, and 36.0 μM) at 25 °C for 30 min before separation at 4 °C. Lanes 1 and 10 are SC(1–660) and frag D controls, respectively. frag D, frag D, fibrinogen fragment D; SC, staphylocoagulase.

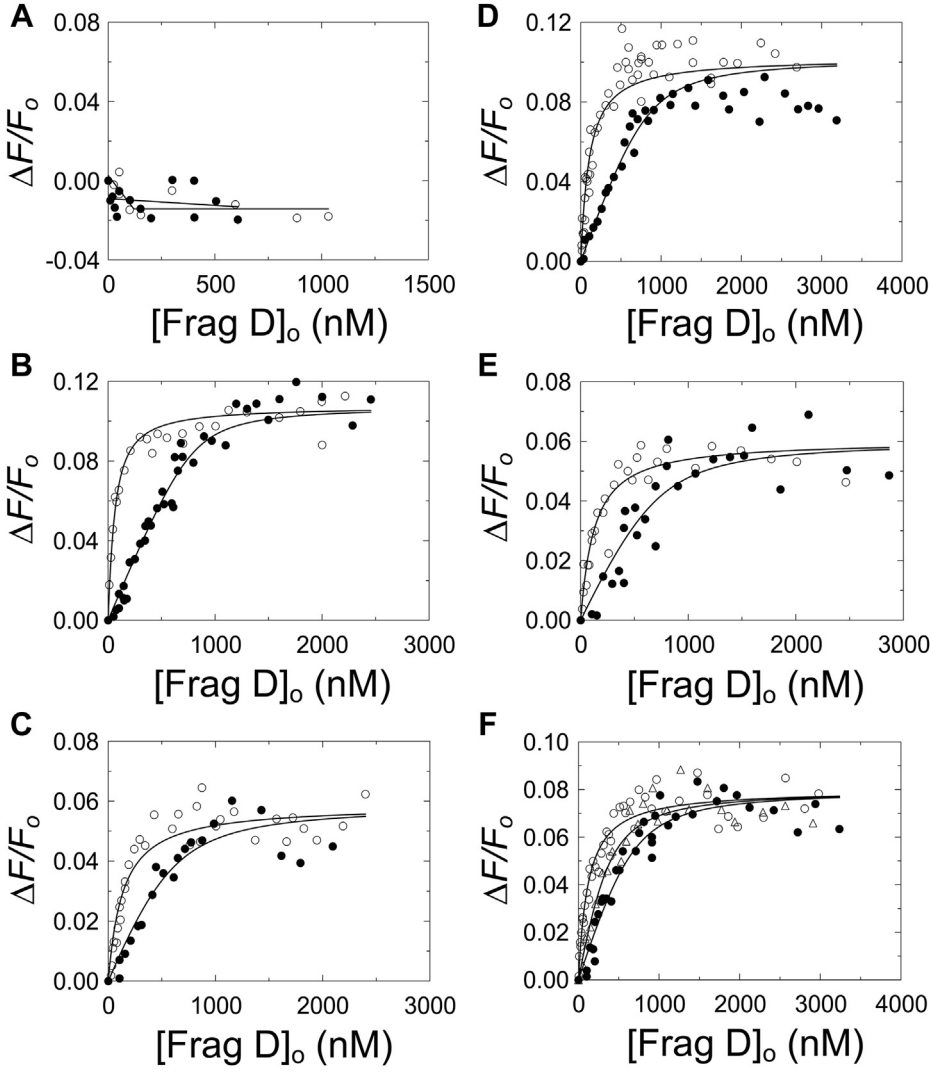

Figure 4. Fluorescence equilibrium binding of repeat constructs to frag D. *A,* titrations of 101 nM [5F]PR (○) and 67 nM [5F]R1 (●) with frag D. *B,* titrations of 25 (○) and 757 (●) nM [5F]PR–R1 with frag D. *C,* titrations of 9 (○) and 690 (●) nM [5F]PR–R2 with frag D. *D,* titrations of 9 (○) and 713 (●) nM [5F]PR–R3 with frag D. *E,* titrations of 21 (○) and 908 (●) nM [5F]PR–R6 with frag D. *F,* titrations of 15 (○), 39 (●), and 848 (Δ) nM [5F]PR–R7 with frag D. *Solid black lines* represent the quadratic fit. Titrations and data fitting were performed as described in the "Experimental procedures" section. The parameters are given in Table 1. frag D, fibrinogen fragment D; PR, pseudorepeat; R, repeat.

multiple frag D molecules at the C-terminal SC domain. In incubations of 2.5 μM [5F]ProT with 3.75 μM SC, [5F]ProT binding was saturated because of the tight K_D of this interaction. Subsequent incubation of the complex with molar excess frag D yielded higher order complexes (Fig. S3, *A* and *B*). All the [5F]ProT was bound in the SC(1–660)·[5F]ProT binary complex, with 1:1 M stoichiometry (lane 3). Binding to multiple frag D molecules occurred, with unbound frag D observed at eightfold molar excess (lane 9).

Frag D bound to [5F]PR–(R1 → R7) containing all seven repeats in order (Fig. S4, *A* and *B*). Higher order complex formation was indicated by an upward shift of fluorescence and Coomassie-stained bands with increasing frag D. Unbound frag D appeared at an approximately eightfold molar excess (lane 7), suggesting a binding stoichiometry of ∼7.

Frag D bound to [5F]PR–R1R6R7 and [5F]PR–R1R2R3, suggesting the presence of binding sites bridging continuous and noncontinuous repeat sequences, and a binding role of conserved residues contained in the bridging areas, independent of the order of the repeats (Figs. S5 and 11). Unbound frag D was observed above 3.5-fold molar excess, suggesting binding of ∼3 frag D molecules per construct, consistent with binding sites formed at the PR–Rx and Rx–Ry junctions.

Equilibrium binding of [5F]-labeled C-terminal repeat peptides to frag D

No increase in fluorescence intensity was observed when [5F]PR and [5F]R1 were titrated with frag D, suggesting that these peptides do not bind frag D (Fig. 4*A*), consistent with our native PAGE findings. In contrast, [5F]PR–R1, [5F]PR–R2, [5F]PR–R3, [5F]PR–R6, and [5F]PR–R7 bound to frag D, with 1:1 stoichiometry and dissociation constants (K_D) ranging from ∼49 to ∼130 nM (Fig. 4, *B–F*). The results for [5F]PR–R1 were in excellent agreement with our previously reported K_D of 36 ± 8 nM for frag D binding (15). The K_D values, $\Delta F_{max}/F_o$,

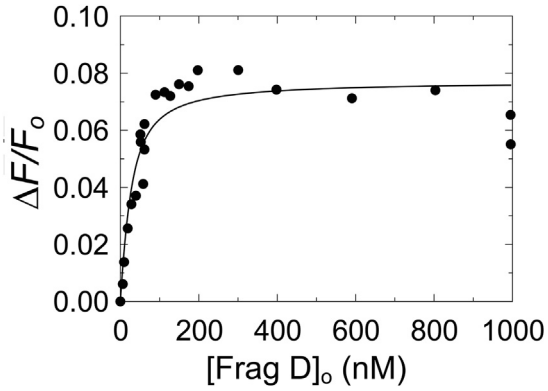

Figure 5. Fluorescence equilibrium binding of [5F]PR–R1 to frag D in the presence of Gly-Pro-Arg-Pro (GPRP). The change in fluorescence intensity ($\Delta F/F_o$) of 19 nM [5F]PR–R1 as a function of total frag D concentration ([frag D]$_o$). The *solid black line* represents the quadratic fit. Titrations and data fitting were performed as described in the "Experimental procedures" section. frag D, fibrinogen fragment D; PR, pseudorepeat; R, repeat.

and stoichiometries obtained by quadratic fit are listed in Table 1. Errors are given by 2× SD (95% confidence interval). The results indicate the presence of one single binding site for frag D that bridges PR and the individual Rx repeats. Because R4 and R5 are identical to R2, their PR–Rx constructs were not tested for frag D binding. Frag D is a trimer of three polypeptide chains, α, β, and γ. The β and γ chains contain holes at their C-terminal end. The peptide Gly-Pro-Arg-Pro (GPRP) is known to bind and block the β-holes and γ-holes of Fbg and frag D (31–33). [5F]PR–R1 was titrated with frag D at saturating GPRP. In the presence of 5 mM GPRP, [5F]PR–R1 still bound frag D with K_D of 18 ± 10 nM, and $\Delta F_{max}/F_o$ 0.08 ± 0.01 (Fig. 5), indicating that [5F]PR–R1, and most likely also the other PR–Rx constructs do not bind the β-chain and γ-chain holes of frag D, but utilize a different binding site on frag D, and that the SC C-terminal domain does not interfere with Fbn polymerization.

NMR assignment of PR–R7, and titration of PR–R7 with frag D

The $^{1}H^{15}N$ heteronuclear single quantum coherence (HSQC) spectrum with the assignments of all PR–R7 residues, including the additional N-terminal and C-terminal residues, was recently published (27). Chemical shift data are retrievable from the Biological Magnetic Resonance Data Bank databank (http://www.bmrb.wisc.edu) under accession number 27036.

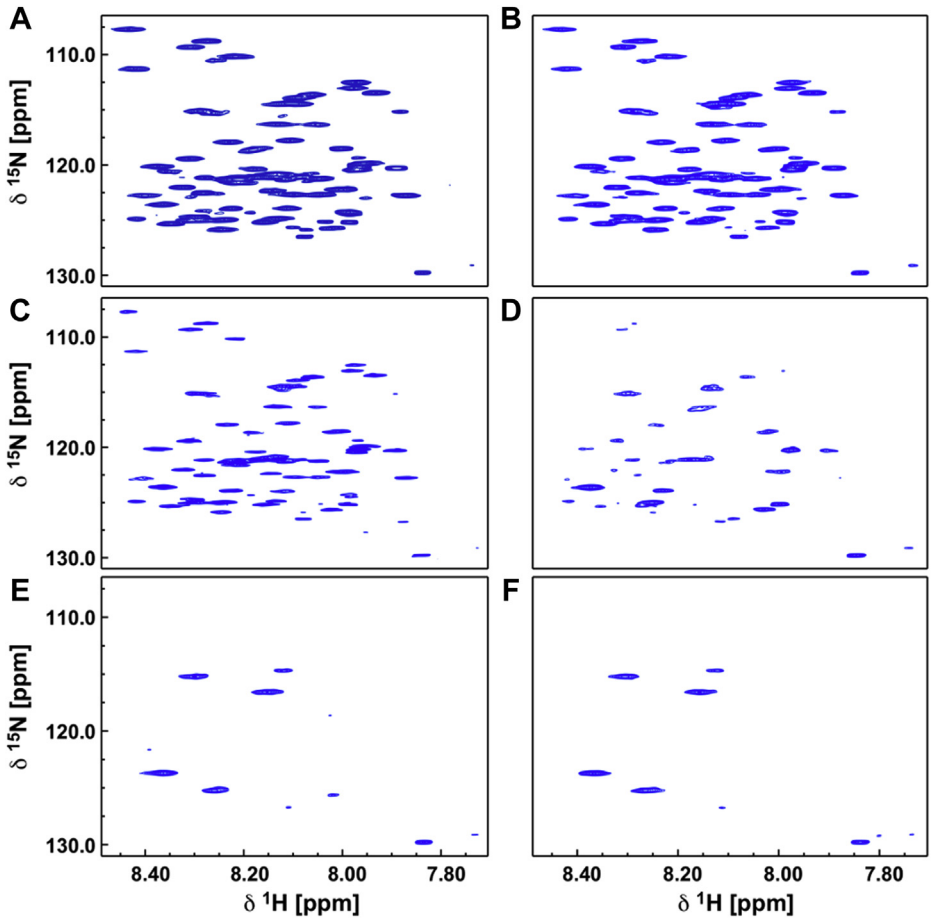

Figure 6. NMR titration of PR–R7 with frag D. The HSQC spectra of ^{15}N-labeled PR–R7 peptide were collected at 600 MHz and 298 K. Increasing amounts of unlabeled frag D were added, and an HSQC was measured with the same parameters, yielding spectra *A* through *F* representing the reference spectrum, with no frag D added in *A*, and 0.5, 1.0, 2.0, 3.21, and 4.95 me of frag D present in spectra *B* through *F*. The spectra clearly show the diminishing peak intensity upon increasing frag D addition, indicating intermediate exchange and complex formation with frag D. frag D, fibrinogen fragment D; HSQC, heteronuclear single quantum coherence; me, mol-equivalent; PR, pseudorepeat; R, repeat.

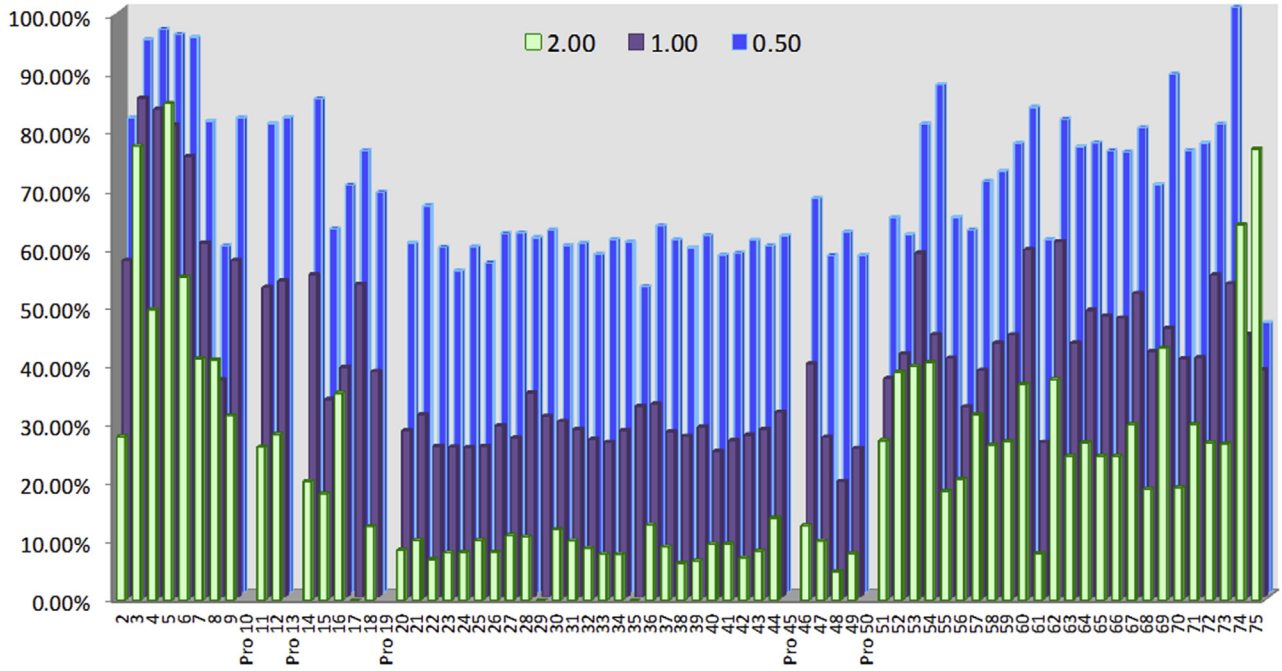

Figure 7. Residue-specific response of PR–R7 in the NMR titration with frag D. *Blue bars* represent the residual percent intensity of the HSQC correlation peak for the respective residue at 0.5 M equivalent frag D; *purple* at 1 M equivalent, and *green* at 2 M equivalent. The intensity is based on the reference spectrum of 65 μM of ^{15}N-labeled PR–R7 peptide alone. Aliquots of 240 μM frag D stock solution were added to achieve the 0.5, 1.0, and 2.0 me conditions. The residue numbering includes the additional N-terminal and C-terminal sequences. frag D, fibrinogen fragment D; HSQC, heteronuclear single quantum coherence; me, mol-equivalents; PR, pseudorepeat; R, repeat.

The assignment for each correlation peak in the ^{1}H–^{15}N HSQC spectrum provides residue-specific information on an atomic level for each amide in the peptide. This allows observation of residue-specific changes of PR–R7 exposed to frag D and results in a clearly defined interaction map. Full assignment was achieved with amide-based experiments, supplemented with novel ^{13}C-direct detect methods, allowing for full N, NH, and C′ resonance assignments, with the exception of the N-terminal and C-terminal one (27). The ^{13}C direct detect experiments allowed to unambiguously assign residues that were problematic in amide-based experiments, such as prolines; Glu^{2}, Thr^{3}, Tyr^{24}, Tyr^{34}, Arg^{44}, and Val^{72} because of heavy peak overlap; low-intensity peaks for His^{8}, Asn^{16}, Asn^{54}, His^{61}, Ala^{62}, and Ser^{70}; and Tyr^{9} as it was between the unassigned His^{8} and Pro^{10}, and therefore, no connections could be assigned (Fig. S6). Peak overlap and low-intensity peaks remained an issue for the analysis of the HSQC-based titration experiments, but unambiguously knowing the exact position of these peaks from the ^{13}C direct detect experiments was crucial during the refinement of the titration analysis. Given the very limited chemical shift dispersion of 8.2 ± 0.27 ppm in the proton dimension, which led to the peak overlap, it was anticipated that the PR–R7 peptide had limited to no secondary structure. With the backbone assignment in hand, secondary structure prediction using the program Talos+ (34) confirmed that there was no consistent secondary structure to be anticipated in PR–R7 alone (Fig. S7).

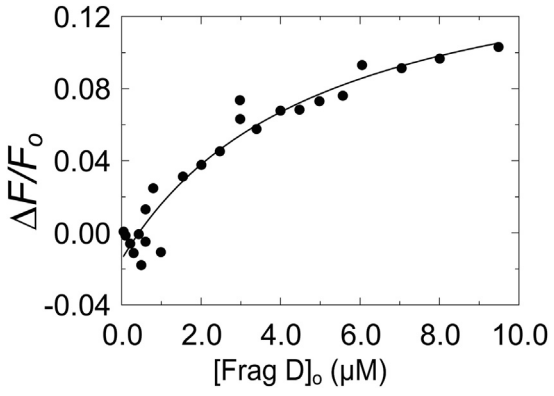

Figure 8. Fluorescence intensity titration of [5F]MP with frag D. Change in fluorescence intensity ($\Delta F/F_o$) of 23 nM [5F]MP as a function of total frag D concentration ([frag D]$_o$). The *solid black line* represents the quadratic fit. Titrations and data fitting were performed as described in the "Experimental procedures" section. frag D, fibrinogen fragment D; MP, minimal peptide.

With the HSQC spectrum assigned, binding of frag D to PR–R7 was investigated in sodium phosphate buffer (pH 7.0). The initial spectrum contained 65 μM of ^{15}N-labeled PR–R7 peptide alone and exhibited all expected nitrogen–proton resonances. Upon successive addition of aliquots from a 240 μM stock solution of nonlabeled frag D, most resonances became weaker as more frag D was added (Fig. 6). Individual titration points were chosen at 0.5, 1.0, 2.0, 3.21, and 4.95 mol-equivalents (me) of frag D to PR–R7 peptide. Decreasing intensity of most resonances in the HSQC spectrum was attributed to intermediate exchange, and formation of a complex, affecting the correlation time of the molecule substantially broadening those resonances. The titration was analyzed by measuring the peak intensity for each residue of

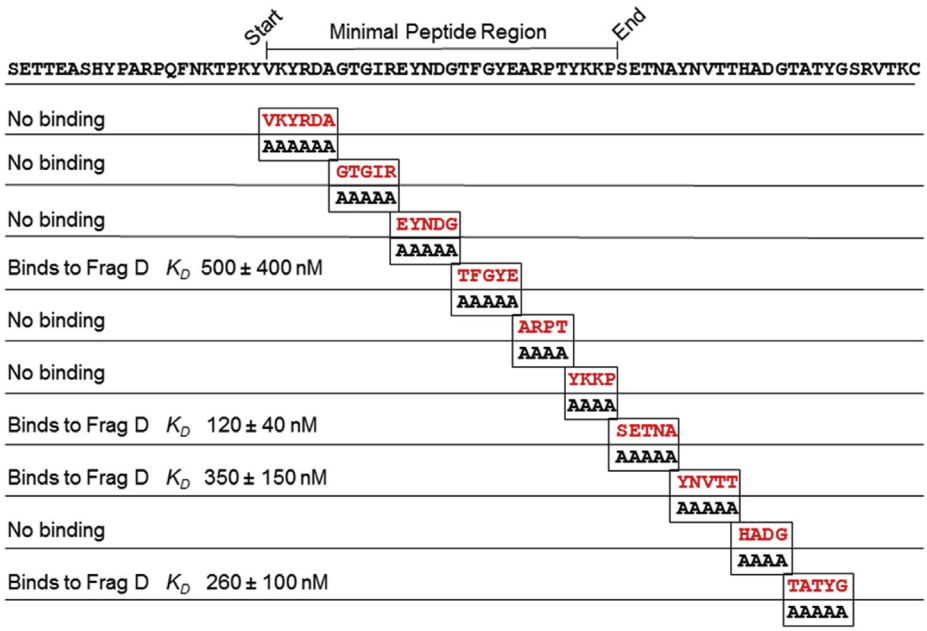

Figure 9. Binding of frag D to PR–R7 alanine mutants. Alanine scanning mutagenesis of the MP region and the remainder of the R7 C-terminal region. The constructs contain the additional N-terminal SETTEASHYP and C-terminal SRVTKC sequences. The MP consists of a continuous stretch of 29 residues of which 21 are in the PR and eight in R7. frag D, fibrinogen fragment D; MP, minimal peptide; PR, pseudorepeat; R, repeat.

the first three titration spectra, recording them as a percentage of the reference spectrum (Fig. 7). The peak intensity change follows the same trend for each individual residue after each addition of frag D. Only the first three titration points at 0.5, 1.0, and 2.0 me of frag D contained meaningful information for the majority of residues and were analyzed. At higher frag D concentrations, most resonances were exchange broadened or affected by the slower tumbling of the larger frag D·PR–R7 complex to the point where individual peaks were no longer contributing in a relevant matter to the analysis. Only about a dozen high-intensity peaks remained visible in the spectra with 3.21 and 4.95 me of frag D. Manual analysis of overlapping peaks assured correct intensity representation. HSQC spectra of residue pairs Glu^{2}-Tyr^{9}, Ser^{7}-Thr^{53}, Lys^{20}-Asp^{26}, Tyr^{34}-Phe^{39}, and Glu^{33}-His^{61} were overlapping, with mutual influencing of peak intensities, which complicated independent analysis. The Glu^{2}-Tyr^{9} and Glu^{33}-His^{61} pairs merited further analysis. Glu peaks, typically weak to begin with, are often exchange broadened in these spectra. The normally stronger Tyr^{9} was weakened by frag D binding, making it look similar to the Glu^{2} peak. Similarly, Glu^{33} was in addition broadened by its position in the binding interface, whereas the overlapping His^{61} was exchange broadened from the beginning, and this effect is accentuated in this environment, causing the intensities of these two peaks to decrease at similar rates. Figure 7 shows that the intensity of Glu^{2} and His^{61} is clearly smaller than anticipated compared with their neighbors, whereas Tyr^{9} and Glu^{33} fit in well with their neighbors, indicating that the intensity fit indeed was correct for those residues, but for different reasons. The intensities of other overlapping peaks matched well with those of their neighbors and had no impact on the overall interpretation. The correlation peaks in the HSQC spectrum at 2.0 me of frag D for Lys^{17}, Thr^{29}, and Asn^{35} were no longer detectable, but the first two titration points showed clear signal intensities that were analyzed. More interestingly, Figure 7 reveals a trend where the stretch of residues 20 to 49 shows consistently more diminished signal intensity in all three titration points, compared with the C-terminal residues 51 to 75 and N-terminal residues 2 to 18 that retain a stronger intensity on average. The N-terminal residues three to seven are affected the least, and their signals remain visible even at the highest frag D addition. The most plausible explanation is that frag D has its main binding interaction with PR–R7 within the PR–R7 residues 20 to 49, which suggests a binding site overlapping PR and R7. Significantly less signal reduction was observed for the peaks in the C-terminal residues 51 to 75 leading to the conclusion that this portion of the peptide might contribute less to the interaction with frag D, although weak binding of that sequence with frag D can still be anticipated. The stretch of residues from 22 to 50 was determined to constitute the MP that is required for binding to frag D. Because the NMR studies required 20 mM sodium phosphate, 150 mM NaCl, pH 7.0 buffer, equilibrium binding of frag D to [5F]PR–R7 was also performed in phosphate buffers with corresponding ionic strength at pH 7.0 and 7.4 to determine whether the phosphate buffer and pH affect binding. Titration of [5F]PR–R7 with stoichiometries fixed at 1, yielded K_D values of 3 ± 2 μM and 27 ± 75 nM at pH 7.0 and 7.4, respectively. The data at pH 7.4 corresponded well with the results for frag D binding in Hepes buffer. Titrations in phosphate buffer were somewhat noisier than in Hepes buffer, presumably because of probe–buffer interactions. Equilibrium binding of labeled PR–R7 at pH 7.0 was weaker, possibly because of the combination of differences in protonation states of the two His imidazole groups (35) in this construct, and the fluorescein probe with a pK_a of 6.4.

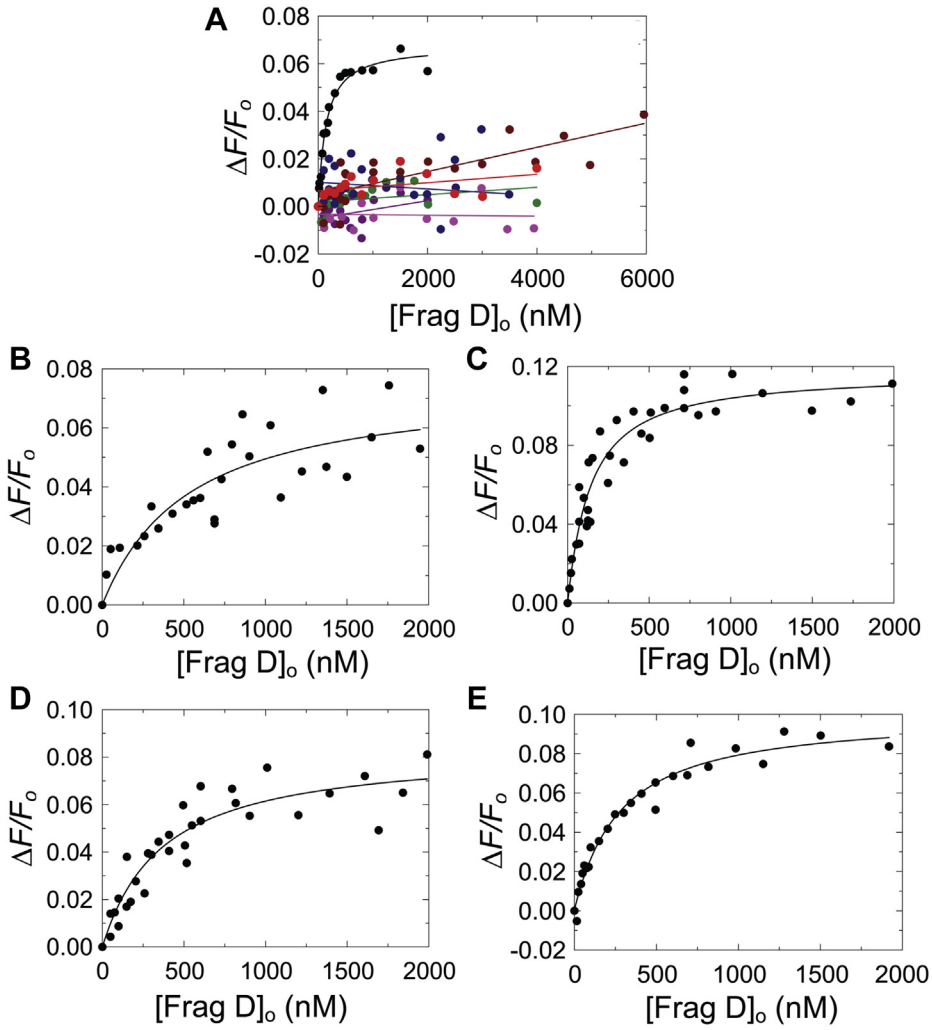

Figure 10. Equilibrium binding of frag D to [5F]PR–R7 alanine mutants. *A,* the change in fluorescence intensity ($\Delta F/F_o$) of 19 nM [5F]PR–R7 (•), 33 nM [5F]PR–R7-VKYRDA (*red*), 39 nM [5F]PR–R7-GTGIR (*black*), 35 nM [5F]PR–R7-EYNDG (*blue*), 18 nM [5F]PR–R7-ARPT (*brown*), 24 nM [5F]PR–R7-YKKP (*green*), and 29 nM [5F]PR–R7-HADG (*pink*) as a function of total frag D concentration ([frag D]$_o$). *B,* $\Delta F/F_o$ of 37 nM [5F]PR–R7-TFGYE as a function of [frag D]$_o$. *C,* $\Delta F/F_i$ of 27 nM [5F]PR–R7-SETNA as a function of [frag D]$_o$. *D,* $\Delta F/F_o$ of 27 nM [5F]PR–R7-YNVTT as a function of [frag D]$_o$. *E,* $\Delta F/F_o$ of 27 nM [5F]PR–R7-TATYG as a function of [frag D]$_o$. *Solid lines* represent the quadratic fit. Titrations and data fitting were performed as described in the "Experimental procedures" section. frag D, fibrinogen fragment D; PR, pseudorepeat; R, repeat.

However, our NMR titration of the labeled peptide, collected at micromolar reactant concentrations, clearly indicated a distinct region of interaction under these experimental conditions.

Equilibrium binding of frag D to the 5F-labeled MP, [5F]MP

The 29-residue MP, identified by NMR studies, was synthesized, with an additional C-terminal Cys for attachment of a 5F probe. Titration of [5F]MP (23 nM) with frag D demonstrated binding, with K_D of 5 ± 4 μM, $\Delta F_{max}/F_o$ 0.17 ± 0.02, and a fixed stoichiometry of 1 (Fig. 8). This indicates that the MP sequence is sufficient to bind frag D.

Equilibrium binding of Ala scanning mutants of PR–R7 to frag D

Ala scanning mutagenesis and equilibrium binding further determined the specific PR–R7 residues involved in frag D binding. Sequential mutation of four to six amino acid residue stretches was done in the MP region and beyond, until the end of repeat R7. 10 Ala mutant constructs of [5F]PR–R7 were titrated with frag D. Ala mutants of VKYRDA, GTGIR, EYNDG in PR, and of ARPT, YKKP, and HADG in R7 abolished binding (Figs. 9 and 10*A*), indicating essential contributions of these sequences to frag D binding. VKYRDA, GTGIR, and EYNDG form a contiguous stretch located at the C-terminal region of the PR. ARPT and YKKP are located at the N-terminal region of R7, whereas HADG is located toward the C terminus of R7. Mutations at TFGYE, SETNA, YNVTT, and TATYG still allowed binding of frag D, with respective K_D values of 500 ± 400, 120 ± 40, 350 ± 150, and 260 ± 100 nM (Figs. 9 and 10, *B–E*). Ala substitution at SETNA resulted in a binding affinity similar to that of [5F]PR–R7, suggesting limited involvement of these residues in binding. Maximum fluorescence intensity increases of these four constructs were comparable to that of native [5F]PR–R7. The sequence

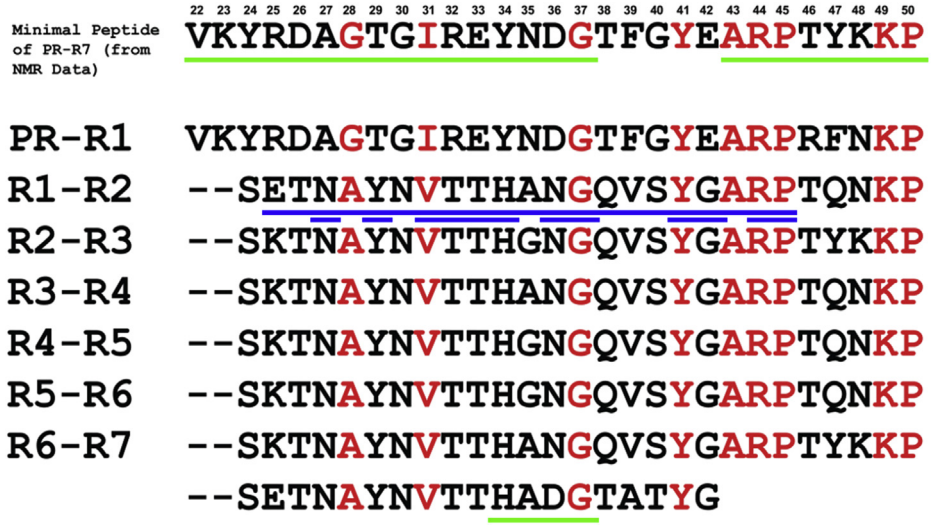

Figure 11. MP sequence alignment with the bridging sequences between SC repeats. The alignment shows the conserved residues (*red*) at positions G^{37}, Y^{41}, A^{43}, R^{44}, P^{45}, K^{49}, and P^{50}. The residues G^{28} and I^{31} are present only in the PR and are replaced with similar size hydrophobic residues A and V in other repeats. Residue numbering in the MP is consistent with the PR–R7 construct including additional N-terminal and C-terminal residues, as used in the NMR experiments. The last line in the figure is the remainder of R7. Sequences of putative interactions with frag D molecules, identified by Ko, are underlined in *blue* (Coa-RI sequence and individual Ala residue scanning). Our Ala-scanned sequences are underlined in *green*. frag D, fibrinogen fragment D; MP, minimal peptide; PR, pseudorepeat; R, repeat; SC, staphylocoagulase.

alignment of the corresponding MP regions in other inter-repeat regions showed strictly conserved G^{37}, Y^{41}, A^{43}, R^{44}, P^{45}, K^{49}, and P^{50} (Fig. 11). G^{28} and I^{31} are present only in the PR, and the corresponding residues A and V in other repeats are hydrophobic and similar in size. Y^{41} is highly conserved; however, Ala substitution still allows for weak binding of frag D.

Clotting of Fbg by the SC(1–325)·ProT^{QQQ} and SC(1–660)·ProT^{QQQ}* complexes*

Cleavage of Fbg to Fbn causes turbidity increase because of formation and polymerization of Fbn with a lower solubility. We compared the rates of Fbn clotting by T, and the active SC(1–325)·ProT^{QQQ*} and SC(1–660)·ProT^{QQQ*} complexes. ProT(R155Q,R271Q,R284Q), or ProT^{QQQ}, is a human ProT variant with its prothrombinase and T cleavage sites mutated to prevent proteolytic processing (36). It can be activated proteolytically to a meizothrombin form as well as conformationally by triggering formation of an active site by occupation of its Ile^{16} pocket by the N terminus of SC. T, as a control reaction, initiated immediate cleavage of Fbg, whereas addition of ProT^{QQQ} in mixtures with SC(1–325) and SC(1–660) showed a lag phase during which the SC(1–325)·ProT^{QQQ*} and SC(1–660)·ProT^{QQQ*} complexes are formed (Fig. 12). In the T-initiated or SC(1–325)·ProT^{QQQ*}-initiated cleavage of Fbg at 0.5 mg/ml, there was rapid and comparable increase in turbidity reaching a maximal level, indicating clot stabilization. Clot formation by SC(1–660)·ProT^{QQQ*} was slower, and the initial rates of turbidity increase, and absorbance readings at clot stabilization were dependent on the Fbg concentration. SC(1–325) conformationally activates ProT but lacks the C-terminal domain for frag D binding. This additional interaction of SC(1–660) may sequester Fbg molecules at the C-terminal domain, thereby decreasing the effective *in vitro* Fbg concentration available for cleavage by SC(1–660)·ProT^{QQQ*} or posing conformational restrains on cleavage of Fbg bound in the substrate mode, either with or without simultaneous tethering to the SC repeat domain.

Table 1
Parameters of [5F]PR, [5F]R1, and [5F]PR–R binding to frag D

Repeat construct	Stoichiometric factor (mol frag D/mol repeat) (n)	K_D (nM)	$\Delta F_{max}/F_o$
[5F]PR	No binding		
[5F]R1	No binding		
[5F]PR–R1	1.0 ± 0.1	49 ± 14	0.11 ± 0.01
[5F]PR–R2	0.9 ± 0.2	130 ± 42	0.06 ± 0.01
[5F]PR–R3	1.1 ± 0.2	99 ± 26	0.10 ± 0.01
[5F]PR–R6	0.8 ± 0.2	115 ± 47	0.06 ± 0.01
[5F]PR–R7	0.8 ± 0.2	112 ± 25	0.08 ± 0.01

Dissociation constants (K_D), stoichiometric factors (n), and maximum fluorescence intensity ($\Delta F_{max}/F_o$) were obtained by fitting of the titration data by the quadratic binding equation. Experimental errors represent ±2 SD. Equilibrium binding was performed as described under the "Experimental procedures" section.

Fluorescence anisotropy titrations of repeat constructs binding to frag D

The full-length repeat construct, PR–(R1 → R7), contains the highly conserved PR and seven repeats, of which R2, R4, and R5 are identical. Constructs for direct or competitive binding, compared with full-length SC(1–660), are shown in Figure 1. Using fluorescence anisotropy, we titrated three independently prepared batches of [5F]PR–(R1 → R7) with frag D. Their [5F]PR–(R1 → R7)·frag D complexes were used in competitive titrations with three independently prepared PR–R1R2R3 batches to determine K_D values for PR–R1R2R3 and to validate the assay and reproducibility. We performed competitive titrations of the [5F]PR–(R1 → R7)·frag D complex with PR–R1R6R7, PR–R3R4R7, and PR–R3R6R7

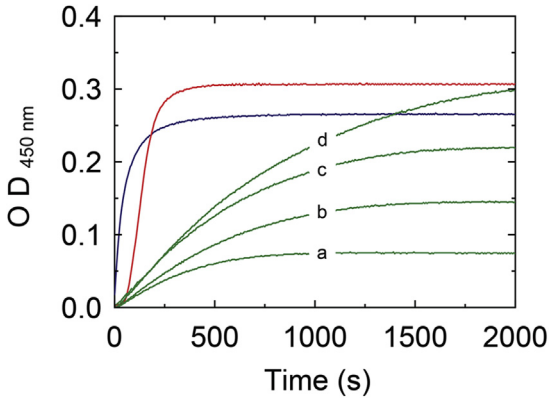

Figure 12. Turbidity assay of Fbg cleavage. Increase in turbidity at 450 nm, 25 °C for mixtures of 10 nM thrombin with 0.5 mg/ml Fbg (*blue*); 10 nM SC(1–325)·ProT^{QQQ*} complex with 0.5 mg/ml Fbg (*red*); and 10 nM SC(1–660)·ProT^{QQQ*} complex with increasing Fbg (*green*, *A–D*; 0.3, 0.5, 0.75, and 1.0 mg/ml, respectively). Fbg, fibrinogen; ProT, prothrombin; SC, staphylocoagulase.

measured by fluorescence anisotropy. Interbatch results were in good agreement, with stoichiometries of ∼5 for frag D binding to [5F]PR–(R1 → R7), K_Ds of ∼7 to 32 nM, maximum anisotropy changes r_{max} of 0.13 to 0.15, and r_0 initial anisotropy of ∼0.1 (Figs. 13 and S8; Table 2). Competitive binding of frag D to PR–R1R2R3, PR–R1R6R7, PR–R3R4R7, and PR–R3R6R7 gave stoichiometries of ∼3 as expected for a construct containing three inter-repeat sequences with conserved residues essential for frag D binding and binding parameters comparable to those of [5F]PR–(R1 → R7). Swapping of the repeat order did not affect the position of critical and conserved residues in sequences bridging the repeats and did not weaken the binding of frag D significantly.

CD spectroscopy of SC repeat peptides and frag D

CD spectroscopy of full-length SC(1–660) (*blue*), SC(1–325) (*brown*), PR–R7 (*black*), PR–(R1 → R7) (*red*), and frag D (*green*) was performed to determine the presence of secondary structure content (Fig. S9). Frag D showed major helical content with typical minima at 208 and 222 nm. The negative band at 224 nm in the SC(1–325) spectrum was suggestive of helix (37), consistent with its known crystal structure (19). The profiles of PR–R7, PR–(R1 → R7), and SC(1–660) indicated an extended or irregular structure. The 222/208 nm ratio of >1.1 for frag D suggested the presence of coiled-coil helices, consistent with its published structure (32). However, the PR–(R1 → R7) spectrum was more ambiguous, with a positive band at 212 nm suggesting random coil (38, 39). Although the 222/208 nm ratio was >1, secondary structure predictions by GOR IV (40) and PSIPRED (41) gave ∼70% random coil and ∼30% extended strand content for PR–(R1–R7) and PR–R7, with no helical content. The prediction based on the NMR data confirms the calculations and indicates no presence of secondary structure (Fig. S7). The respective helix, extended

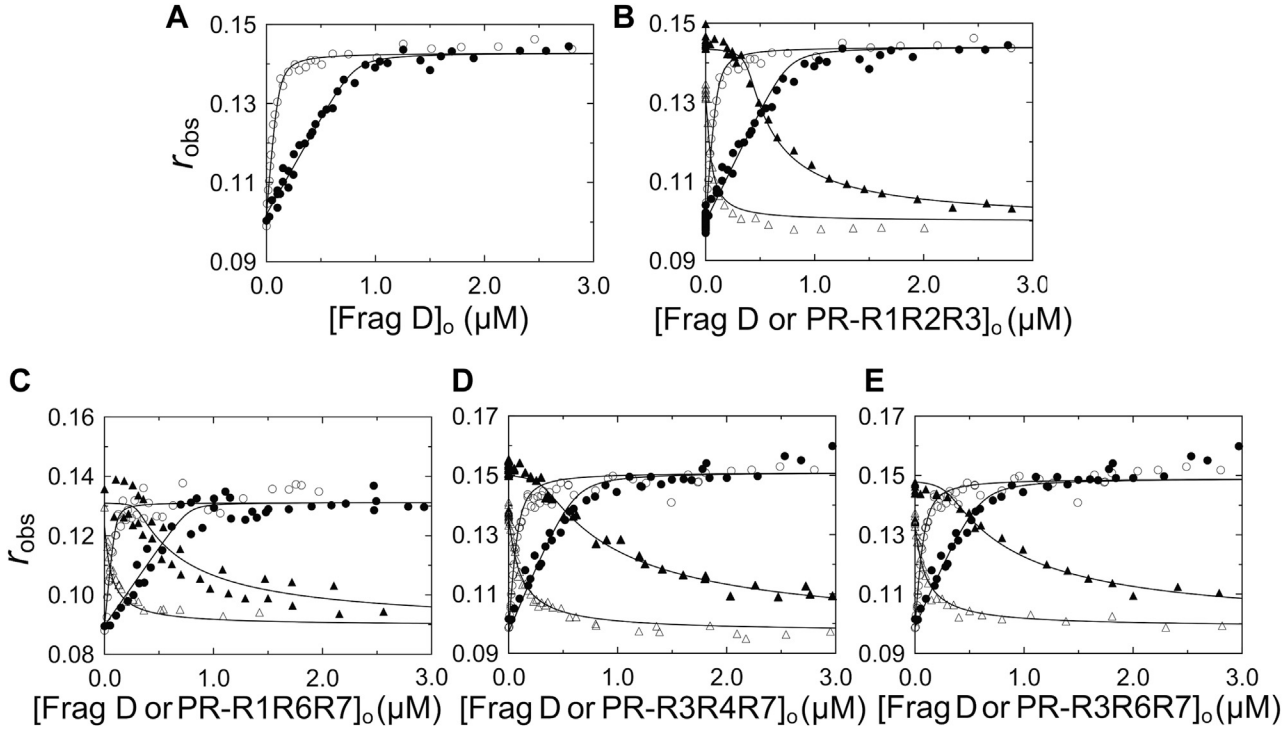

Figure 13. Fluorescence anisotropy titrations of repeat constructs binding to frag D. *A*, observed anisotropy (r_{obs}) of 21 (○) and 154 (●) nM [5F]PR–(R1 → R7) as a function of total frag D concentration ([frag D]$_o$). *B*, simultaneous fit of *A* with competitor PR–R1R2R3 titrated into mixtures of 21 nM [5F]PR–(R1 → R7) with 105 (Δ) and 1053 (▲) nM frag D; *C*, simultaneous fit of frag D titration of 21 (○) and 155 (●) nM [5F]PR–(R1 → R7) and competitor PR–R1R6R7 titration into mixtures of 21 nM [5F]PR–(R1 → R7) with 107 (Δ) and 959 (▲) nM frag D. *D*, simultaneous fit of frag D titration of 16 (○) and 120 (●) nM [5F]PR–(R1 → R7) and competitor PR–R3R4R7 titration into mixtures of 16 nM [5F]PR–(R1 → R7) with 107 (Δ) and 1008 (▲) nM frag D. *E*, simultaneous fit of frag D titration of 16 (○) and 120 (●) nM [5F]PR–(R1 → R7) and competitor PR–R3R6R7 titration into mixtures of 16 nM [5F]PR–(R1 → R7) with 99 (Δ) and 992 (▲) nM frag D. Titrations and data analyses were performed as described under the "Experimental procedures" section. *Solid black lines* represent the quadratic (*A*) and cubic binding fits (*B–E*). Binding parameters are given in Table 2. frag D, fibrinogen fragment D; PR, pseudorepeat; R, repeat.

Table 2
Binding parameters from titrations of repeat constructs with frag D

Repeat construct	Stoichiometric factor (mol frag D/mol repeat) (n)	K_D (nM)	r_{max}	r_o
PR–R1R2R3	3.3 ± 0.4	25.0 ± 8.0	0.15 ± 0.01	0.10 ± 0.01
	3.5 ± 0.8	7.0 ± 6.0	0.13 ± 0.01	0.09 ± 0.01
	2.5 ± 0.3	7.0 ± 3.0	0.14 ± 0.01	0.10 ± 0.01
PR–R1R6R7	3.0 ± 0.7	8.0 ± 9.0	0.13 ± 0.01	0.09 ± 0.01
PR–R3R4R7	2.8 ± 0.6	42.0 ± 16.0	0.15 ± 0.01	0.10 ± 0.01
PR–R3R6R7	3.0 ± 0.8	42.0 ± 21.0	0.15 ± 0.01	0.10 ± 0.01
[5F]PR–(R1 → R7)	5.2 ± 0.3	12.0 ± 5.0	0.14 ± 0.01	0.10 ± 0.01
	4.8 ± 0.6	7.4 ± 6.0	0.13 ± 0.01	0.09 ± 0.01
	5.1 ± 0.5	32.0 ± 9.0	0.15 ± 0.01	0.10 ± 0.01

Three independent [5F]PR–(R1 → R7) preparations were titrated with frag D, and the dissociation constant (K_D), stoichiometric factor (n), initial anisotropy (r_o), and maximum anisotropy (r_{max}) were obtained by fitting to the quadratic binding equation. Competitive binding of PR–R1R2R3 (three independent preparations), PR–R1R6R7, PR–R3R4R7, and PR–R3R6R7 to frag D was measured by titration of two fixed [5F]PR–(R1 → R7)/frag D mixtures with the unlabeled peptides. The two curves of each dataset were fit simultaneously with the two direct [5F]PR–(R1 → R7) binding curves, using the cubic equation, to obtain K_D and n for the competitor peptides. Experimental error represents ±2 SD. Binding studies and data analysis were performed as described under the "Experimental procedures" section.

strand, and random coil content estimates for SC(1–660) were 26, 20, and 54% (GOR IV) and 28, 12, and 60% (PSIPRED); and for SC(1–325), 50, 13, and 37% (GOR IV) and 54, 1, and 45% (PSIPRED). Prediction of natural disordered regions in full-length SC(1–660) by PONDR-FIT (42) indicated an overall disordered content of 46.21%, with 75.66% of the R1–R7 sequence identified as disordered.

Discussion

Coagulase-positive *S. aureus* employs various Fbg-binding virulence factors, including SC, to facilitate rapid colonization and spreading inside the human host (43–48). We showed previously that the complex of SC and SC(1–325) with conformationally activated host ProT forms a new binding site for substrate Fbg, distinct from ProT proexosite I, and proteolytically converts it to Fbn clots that serve as focal points for bacterial adhesion (21). In addition, localization of SC on host fibrin(ogen) is facilitated by the SC C-terminal repeat sequence (15, 28, 29, 49). SC serotypes have four to nine highly conserved repeats, preceded by a PR containing a TFGYE sequence not present in the repeats (3, 19, 22, 50) (Figs. 2 and S1). These repeats, in part the result of selective pressure, increase the Fbg-binding efficiency of SC. Our studies used SC of the prototypical Newman D2 Tager 104 strain that has seven repeats, with 100% identical R2, R4, and R5, suggesting duplication in the genome (19).

We used the frag D domain of Fbg/Fbn to demonstrate binding to free and ProT-complexed full-length SC(1–660); C-terminal constructs containing PR and one or more repeats; the MP identified by NMR; and to demonstrate the absence of binding to PR, the single repeats, or specific Ala-scanned PR–R7 constructs. The PR–R constructs with one repeat exhibited similar affinities for frag D, suggesting a fairly conserved binding site, even with minor sequence variability among the repeats. We chose PR–R7, with the highest expression levels, for independent and mutually validating binding approaches because NMR typically requires fairly high experimental concentrations.

We identified the PR sequence VKYRDAGTGIREYNDG, strictly conserved among all serotypes, and ARPTYKKP and its respective similar sequences in the N-terminal portion of the repeats, as essential determinants in frag D binding. The PR sequence differs from the previously identified Fbg-binding Coa-RI sequence (28) and represents a partial novel binding site (Fig. 11). Ala scanning including nine conserved residues in the MP abolished or severely weakened frag D binding to PR–R7, supporting frag D-binding sites at the junctions of PR–R and R–R. HADG at the C-terminal end of PR–R7 aligns with YNDG in the MP, containing the conserved G^{37}. Disruption of frag D binding by Ala substitution of either sequence (Figs. 9 and 10*A*) indicates that this G residue is a part of multiple frag D-/Fbg-binding sites in the C-terminal repeat region. PR and R1 by themselves did not bind frag D with measurable affinity, whereas all the PR–R constructs, containing the conserved G/A^{28}, I/V^{31}, and G^{37} residues aligned in the R–R bridging sequences, bound frag D with a 1:1 stoichiometry and K_D values in the ∼50 to 130 nM range. These findings, together with our Ala scanning results, are consistent with a simultaneous requirement for both binding subsites. Tighter binding of PR–Rx compared with MP suggests multiple binding interactions for frag D, and our findings suggest as many as five to six binding sites, in the complete repeat domain of SC (15). The capacity to bind multiple Fbg/Fbn molecules simultaneously may facilitate bacterial localization on blood clots, evasion of the host immune system (51), and may impair the efficacy of antibiotic therapy.

N-terminal cleavage of the Fbg α-chains and β-chains to form Fbn monomer releases the fibrinopeptides AαBβ, with generation of new Gly-Pro-Arg N termini that, respectively, bind the γ-holes and β-holes to form the Fbn network. The tetrapeptide GPRP binds to Fbg and frag D holes with an affinity of ∼5 mM (31, 32) and is routinely used to prevent Fbn polymerization in solution studies of Fbn monomer. Blocking the frag D holes with GPRP had no weakening effect on its binding to PR–R1 (Fig. 5), excluding them as potential interaction sites. This implies that interaction sites of frag D are located elsewhere in the frag D molecule, possibly in the coiled-coiled region. The modestly tighter affinity for frag D binding (18 nM) compared with that in the absence of GPRP (∼36–49 nM) may reflect a combination of subtle conformational changes and batch-to-batch PR–R1 and frag D variability.

Mapping the fibrinogen-binding site on the SC C terminus

The NMR data further confirmed our hypothesis of a functional binding unit comprised of residues from both PR and the repeats. Decreased NMR peak intensity upon titration with frag D, and residue-specific response showed that the MP, a continuous stretch of 29 amino acids in PR–R7, binds frag D. Residue-specific analysis of the binding interaction between PR–R7 and frag D required initial backbone assignment of this peptide. Very limited dispersion of the NMR signals in the proton dimension raised the suspicion that PR–R7 had limited secondary structure in its apo (unbound) state, which subsequently was shown by the chemical shift prediction using Talos+. This limited dispersion led to substantial signal overlap, and full backbone assignment was ultimately achievable with the aid of novel ^{13}C-direct detect measurements geared toward such peptides. A very careful and manual analysis of the titration experiments ensured true representation of the peak intensities for each residue. Based on these results, it is clear that an important interaction of frag D consists of residues 20 to 49 on PR–R7. The C-terminal end of the interaction site is defined more clearly than the N-terminal end, although Ala scanning identified both to be required for binding. Both ends are flanked by prolines, and at this point, their role at either side of the MP is unclear. Residues 51 to 75 were significantly less impacted by the presence of frag D, but a secondary interaction with those residues cannot be ruled out as indicated by the Ala scan of that portion of PR–R7. The HADG sequence and aligned YNDG/HANG/HGNG in other repeats may actually participate in subsequent R/R binding of frag D/Fbg.

A previous study used SC from *S. aureus* strain 8325-4 (22), with a PR and five repeats, for investigation of C-terminal Fbg interactions (28). ELISA assays and microcalorimetry, respectively, demonstrated Fbg and frag D binding to recombinant fragments of the C-terminal SC repeats. Sequence similarities in the SC PR and R1–R2 junction with another *S. aureus* virulence factor, the extracellular Fbg-binding protein (Efb), suggested a common Fbg binding motif, absent in the virulence factor von Willebrand factor–binding protein that uses another mechanism to recruit Fbg (29). Efb uses Fbg binding to facilitate phagocytosis escape (13), and the pathogen co-opts host Fbg binding by both SC and Efb to evade the host immune system. In ELISA competition assays, short peptides inhibited binding of a C-terminal SC fragment to Fbg-coated microtiter wells. This fragment included the PR and repeats R1 to R5. The competitive peptides were Coa-R0, which has a 32-residue sequence bridging PR and R1; the 27-residue peptides Coa-RI, Coa-RI2, Coa-RI3, and Coa-RI4, all bridging R1 and R2; and Coa-RV1 with a partial R5 sequence. The sequence of repeat R5 in SC 8325-4 largely corresponds to that of repeat R7 in SC Tager 104. Binding of Coa-RV1 to immobilized Fbg and frag D by isothermal titration calorimetry cannot readily be explained by potentially different exposure of frag D epitopes in conformationally heterogeneous immobilized Fbg (52) and in solution. However, three other peptides, Coa-RV2, Coa-RV3, and Coa-RV4 largely corresponding to R5 were not competitive, consistent with our hypothesis that most single repeats may not have a high affinity for frag D. Binding of Coa-R1 and Coa-RI3 to frag D, measured by isothermal titration calorimetry, yielded affinities between ∼77 and ∼140 nM, in agreement with our fluorescence equilibrium binding data for the affinities of labeled PR–R constructs (Table 1). Ala scanning of ET**N**A**Y**N**V**T**TH**A**NG**QVS**Y**-G**A**R**P**TYKKPS bridging R1 and R2 in Coa-RI (28) indicated critical (***bold***, ***underlined***) and important (***bold***) residues. Our NMR analysis and Ala scanning encompassed a different interdomain sequence, comprised of the C-terminal **VKYR**-**DA**G**T**G**I**R**EYNDG**TFG**Y**E residues of the PR, and the N-terminal part **ARPTYKKP**SETN**A**YN**V**TT**HADG**TAT**Y**G of R7. Figure 11 shows the alignment of critical conserved residues in the PR and the repeat junctions (critical Coa-RI and MP residues *underlined in different colors*). HADG is conserved in the last repeat of the serotypes (50), aligns with YNDG in the conserved PR and also with HANG in Coa-RI. Ala scanning of the PR sequence EYNDG^{37} completely abolished fragD binding to PR–R7 (Fig. 9), suggesting that alignment of G^{37} with the conserved G residues in the inter-repeat sequences plays a critical role. PR residues G/A^{28}, I/V^{31}, G^{37}, and Y^{41} are aligned with the C-terminal sequences in the individual repeats. Ko *et al.* (28) identified essential N, Y, T, H, and G residues in SC 8325-4 repeat R1, flanking the aligned PR residues, and these may represent a complementary and conserved binding motif in the repeat junctions. Unexpectedly, Ala scanning of HADG outside the MP region in PR–R7 abolished frag D binding, even though a complete MP sequence was present. In the absence of a crystal structure of the frag D–PR–R7 complex, PSIPRED analysis of the HADG-$(Ala)_4$ mutant does not indicate significant change in propensity for strand or coil structure in this region. However, conformational changes in this coil sequence and the substitution of D by a nonpolar residue may contribute to a change in overall intramolecular or intermolecular contacts of PR–R7, resulting in the loss of frag D binding (K_D ∼112 nM). These potential structural and charge constraints might be absent in the weaker binding (K_D ∼5 μM) of the isolated MP to frag D. Further structural analysis of the construct is required to identify the cause of the lack of binding.

Although competitive ELISA binding to immobilized full-length Fbg may detect additional secondary binding sites for the SC C-terminal repeat region, it is clear that frag D binding represents a major site of interaction on Fbg. Multiple frag D binding to SC may indicate the potential of multiple full-length Fbg binding and a role in establishing conformational interactions that may favor Fbg binding in the substrate mode to the complex of SC and host ProT.

Semiquantitative native PAGE analysis and quantitative fluorescence equilibrium binding titrations suggested stoichiometries for frag D binding largely consistent with the number of inter-repeat sequences containing conserved motifs, that is, ∼3 for the PR–R1R2R3, PR–R1R6R7, PR–R3R4R7, and PR–R3R6R7 constructs, and ∼5 to 7 for PR–(R1 → R7). This small five to seven discrepancy for PR–(R1 → R7) may reflect different conformational binding site constraints under both experimental conditions. Titrations of all PR–R constructs and the MP titration were fit very well by the 1:1 binding model,

whereas higher order interactions exhibited a typical stoichiometric titration shape and could only be fit satisfactorily by an unconstrained stoichiometry parameter. Equations for the direct and competitive binding analysis are given in Figure S11. The K_D values for frag D binding to the repeat constructs represent affinities based on the assumption of independent and noncooperative binding. K_D values ranged from ∼7 to ∼32 nM for constructs containing the naturally occurring PR–R1 sequence and were only marginally higher (∼42 nM) for those containing a PR–R3 sequence. Similarly, modest differences were observed for frag D binding to labeled PR–R1 and PR–R3 constructs containing only one repeat (∼50 and ∼100 nM, respectively, Table 1). Multiple PR–R1R2R3 and [5F]PR–(R1–R7) preparations exhibited acceptable variability in affinities, with good consistency in the stoichiometry and amplitude parameters. This variability is to be expected in nonlinear regression analysis with no constraint imposed on any of the parameters and using multiple independent protein preparations ([5F]PR–(R1 → R7), PR–R1R2R3, and frag D) in direct and competitive titrations. Minor differences in sample preparation and limitations of assay sensitivity and of fitting interactions with high stoichiometry factors may all contribute to this variability. Frag D affinities for constructs with multiple repeats were higher than those for PR–R constructs containing only one inter-repeat sequence, suggesting a cumulative effect. The naturally occurring PR–R1 sequence appears to correlate with modestly tighter binding, and the slight sequence variability of the individual repeats might affect the affinity somewhat. However, binding of frag D to our constructs irrespective of the order of repeats is consistent with the recurring pattern of conserved residues in the inter-repeat regions (Fig. S1).

The frag D subunit is considerably smaller than Fbg/Fbn, and *in vivo* maximizing Fbg/Fbn occupancy of the SC inter-repeat sequences with minimal sterical hindrance may require a highly organized molecular arrangement such as found in Fbn networks. A hypothetical scheme is shown in Figure S10. These networks serve as anchoring points and concealing structures for *S. aureus* to evade the host immune system (28, 53).

The coil or disordered structure of PR–(R1 → R7) may allow sufficient conformational freedom for multiple frag D binding. The much larger fibrin(ogen) molecules might associate with these junctions in staggered arrays and favor transition of the disordered SC repeat domain into more organized complex structures such as seen in Fbn protofibril association. This transition may facilitate formation of Fbn/bacteria vegetations *in vivo*. In solution, Fbg binding may be substoichiometric with regard to the number of inter-repeat sequences and allow for secondary interactions in addition to the frag D domains. Further structural studies are required to characterize these higher order complexes.

Binding multiple ligand molecules is a characteristic property of intrinsically disordered proteins (54) and intrinsically disordered protein regions (55). Our CD analysis showed an extended or random coil secondary structure confirmation (Fig. S9) of PR–R7 and PR–(R1 → R7), and secondary structure prediction of full-length SC identified major intrinsically disordered protein regions in the C-terminal repeat region (40–42). This facilitates binding of multiple ligands, consistent with our observations. Our binding data did not suggest positive or negative cooperativity and were fit very well by simple quadratic- or cubic-binding equations (Fig. S11).

Capturing circulating host Fbg by the C-terminal repeat domain may provide a mechanism of recruiting Fbg for presentation as a substrate of the SC(1–660)·ProT* complex *in vivo*; however, Fbg binding to the complex as a substrate for activated ProT* may occur independently of binding to the C-terminal domain of SC. In turbidity assays of Fbg cleavage (Fig. 12), Fbg cleavage by T (control) and the SC(1–325)·ProT* complex was rapid, compared with Fbn formation by the SC(1–660)·ProT* complex at a similar Fbg substrate concentration (Fig. 12*B*). Binding to the C-terminal SC domain may sequester the available Fbg for cleavage by the SC(1–660)·ProT* complex, resulting in decreased rates compared with those observed for the SC(1–325)·ProT* complex, lacking the C-terminal domain. Rates and amplitudes of Fbn formation by the SC(1–660)·ProT* complex were dependent on the substrate Fbg concentration, consistent with this hypothesis.

In conclusion, we demonstrated a clear correlation between the specific and highly conserved inter-repeat sequences in the C-terminal domain of SC and the stoichiometry of frag D binding to these repeat sequences. We also demonstrated for the first time that the conserved PR sequence contains important fibrin(ogen)-binding motifs. The disordered nature of the C-terminal SC domains may favor identification of conserved linear epitopes for developing therapeutic antibodies to combat *S. aureus*-associated infections. These antibodies may be effective across the complete spectrum of serotypes.

Experimental procedures

Preparation of frag D from human Fbg

Frag D was purified from human Fbg (56), with some modifications. Fbg (400 mg) was dissolved in 150 mM NaCl, 50 mM imidazole buffer, pH 7.2, to a final concentration of 5 to 10 mg/ml and dialyzed against the same buffer. $CaCl_2$ was added to a final concentration of 5 mM. The Fbg solution was treated with 5 mM iodoacetamide for 15 min at room temperature to inhibit crosslinking by trace FXIIIa. Fbg was digested by trypsin (0.01 mg trypsin/mg Fbg) for 4 h at room temperature. The reaction was terminated by adding soybean trypsin inhibitor to a concentration of 0.03 mg/mg Fbg and incubating for 1 h on ice. The digested solution was precipitated by slowly adding ice-cold ammonium sulfate solution to a final concentration of 1.18 M and stirring for 10 min on ice. The solution was centrifuged at 10,600*g* for 1 h at 4 °C, and the pellet was discarded. The supernatant was further precipitated by slowly adding ice-cold ammonium sulfate solution to a final concentration of 1.61 M and stirring for 10 min. The solution was centrifuged for 10,600*g* for 1 h. The pellet was resuspended in 20 mM Tris buffer, pH 8.0, containing 10 μM *D*-Phe-Phe-Arg-chloromethyl ketone (FFR-CK), 10 μM

D-Phe-Pro-Arg-chloromethyl ketone (FPR-CK), and 100 μM 4-benzenesulfonyl fluoride hydrochloride, and dialyzed against the same buffer at 4 °C. The dialyzed solution was loaded onto a pre-equilibrated 1 ml Resource Q column, washed with 10 column volumes of 20 mM Tris buffer, pH 8.0, and eluted with a 20 mM Tris, 0 to 250 mM NaCl gradient, pH 8.0. Fractions containing frag D were pooled and concentrated. The solution was dialyzed against 20 mM sodium phosphate, 150 mM NaCl, pH 7.0 (for NMR); or 50 mM Hepes and 125 mM NaCl buffer, pH 7.4 (all other experiments) and stored at −80 °C until use. The frag D concentration was calculated using M_r 88,000 and absorbance at 280 nm extinction coefficient of 2.08 ml mg^{-1} cm^{-1} (57).

Preparation of SC C-terminal repeat variants

Combination constructs of PR with single and multiple repeats were amplified by PCR from the SC(1–660) gene of *S. aureus* Newman D2 Tager 104 using degenerate and specific primers and cloned into a modified pET 30b(+) (Novagen) expression vector containing an N-terminal His_6 tag followed by a tobacco etch virus (TEV) cleavage site (15, 58) and the SC residues SETTEASHYP preceding PR, to preserve proper folding and binding properties of PR. The constructs ending in R7 included the C-terminal SC sequence SRVTK of our reference construct AY225090.2. PCR was performed in 50 μl reaction mixtures containing ∼10 ng of SC(1–660) template DNA, 1 ng of primer, 0.8 mM dNTPs, and 1 unit of high-fidelity polymerase (Stratagene). An additional C-terminal Cys residue for 5-IAF labeling was introduced by site-directed mutagenesis (QuikChange) in constructs for fluorescence binding, and all sequences were confirmed by DNA sequencing. The constructs were transformed into *Escherichia coli* Rosetta 2 (DE3) pLysS. Positive colonies were identified by DNA sequencing. LB (150 ml containing 0.1 mg/ml of kanamycin) was inoculated with single colonies and cultured overnight. LB media containing 0.1 mg/ml of kanamycin were inoculated (1:40) with the overnight cultures and grown for 2 to 3 h with shaking at 250 RPM and 37 °C until absorbance of 0.6 at 600 nm was reached. After induction with D-lactose (10 mg/ml) and an additional 4 h growth, cells were centrifuged at 5000*g* for 30 min and lysed in 50 mM Hepes, 125 mM NaCl, 1 mg/ml PEG, 1 mM EDTA buffer, pH 7.4, containing 100 μM phenyl methyl sulfonyl fluoride (PMSF), and 10 μM FFR-CK and FPR-CK, by three freeze–thaw cycles in liquid nitrogen. The lysate was centrifuged at 39,200*g* for 45 min, and the constructs were released from the inclusion bodies in the pellet by suspension in the same buffer containing 3 M NaSCN. The solution was centrifuged and dialyzed against 50 mM Hepes, 325 mM NaCl, 50 mM imidazole buffer, pH 7.4 before chromatography on Ni^{2+}–iminodiacetic acid–Sepharose (5 ml), and elution with a gradient of 0 to 500 mm imidazole (19). The N-terminal His_6 tag was removed by incubation with recombinant TEV protease (15, 59, 60). The C-terminal Cys thiol groups of unlabeled peptides for competitive binding were blocked with 5-iodoacetamide. Peptides (2–4 mg) were initially reduced by adding 2 mM DTT for 30 min on ice and further treated with fourfold molar excess iodoacetamide for 2 h in the dark at 20 °C. Excess blocking agent was removed by dialysis against 50 mM Hepes, 125 mM NaCl, and pH 7.4. Because the experimentally determined molar extinction coefficients ε_{280} of the constructs differed by ∼20% from the theoretical values, molar absorptivities ε_{205} of the peptides at 205 nm were determined directly from their amino acid sequence (https://spin.niddk.nih.gov/clore/) and by using measured absorbance at 205 and 280 m, good estimates for $\varepsilon_{280} = \varepsilon_{205}$ (absorbance at 280 nm/absorbance at 205 nm) were obtained (61). The peptide concentrations were determined from the absorbance at 280 nm using molar extinction coefficients ε_{280} of 10,430 M^{-1} cm^{-1} for PR–R1, PR–R2, PR–R3; 11,920 M^{-1} cm^{-1} for PR–R6 and PR–R7; 17,880 M^{-1} cm^{-1} for PR–R1R2R3 and PR–R1R6R7; 19,370 M^{-1} cm^{-1} for PR–R3R4R7 and PR–R3R6R7; and 31,290 M^{-1} cm^{-1} for PR–(R1 → R7).

Purified peptides destined for labeling were reduced with DTT at 1 mM final concentration and dialyzed against 5 mM 2-(*N*-morpholino)ethanesulfonic acid, 150 mM NaCl buffer, pH 6.0, before labeling with 5-IAF. Cysthiol incorporation was measured as described (15). The pH of peptide solutions was raised to ∼7 by addition of 0.1 v 1 M Hepes, pH 7.0, in the presence of a twofold molar excess of 5-IAF. After addition of 0.9 volumes of 100 mM Hepes, 100 mM NaCl buffer, pH 7.0, and incubation for 1 to 2 h at 25 °C, the reaction was quenched by adding DTT to a final concentration of 1 mM. The mixture was centrifuged for 15 min at 20,820*g*. Excess probe was removed by dialysis against 5 mM 2-(*N*-morpholino)ethanesulfonic acid, 150 mM NaCl buffer, and pH 6.0. The labeled peptides were further purified by C-18 (5 μm, 4.6 × 150 mm; Beckman Coulter, Inc) reverse-phase HPLC. Peptides were eluted using a linear gradient of 0.1% TFA and 100% acetonitrile with 0.1% TFA. The absorbance was measured at 205 nm (peptide bond) and 440 nm (5F probe absorbance). Peak fractions corresponding to 205 and 440 nm were pooled and lyophilized. The lyophilized powder was resuspended in water, and the labeling ratio was measured. Incorporation of fluorescein was determined by absorbance at 280 and 498 nm with an absorption coefficient of 84,000 m^{-1} cm^{-1} for fluorescein and an absorbance at 280 and 498 nm ratio of 0.19 in 6 m guanidine, 100 mm Tris–Cl, 1 mm EDTA buffer, pH 8.5 (62), and determined to be 0.75 to 1.1 mol fluorescein/mol of peptide. [5F]PR, [5F]R1, and [5F]MP were synthesized by Anaspec, Inc. The concentrations of [5F]PR, [5F]R1, and [5F]MP were calculated using the molar extinction coefficients ε_{280} 5960, 2980, and 5120 M^{-1} cm^{-1}, respectively, as determined previously (61).

The full-length SC gene SC(1–660) containing a His_6 tag and TEV cleavage site at the N terminus was amplified using specific primers from genomic DNA of *S. aureus* Newman D2 Tager 104 and cloned into the same pET30b(+) vector. His_6-SC(1–660) was expressed in *E. coli* Rosetta 2 (DE3) pLysS and purified on Ni^{2+}–iminodiacetic acid–Sepharose, followed by removal of the His_6 tag by TEV protease cleavage. The concentration of SC(1–660) was measured using an experimentally determined extinction coefficient of 0.989 M^{-1} cm^{-1} and

a molecular mass of 74,390 Da. Our previously prepared SC(1–325) construct was also used in the current study (19, 30).

Expression and purification of ^{15}N PR–R7 peptides

Single colonies of Rosetta 2 (DE3) pLysS containing the PR–R7 construct were inoculated into 100 ml sterile LB media containing 0.1 mg/ml kanamycin and grown overnight at 37 °C with shaking at 250 RPM. Overnight cultures (60 ml) were centrifuged for 15 min, and the pellets were resuspended in 50 ml sterile milliQ water. Sterile flasks containing 900 ml of milliQ water (two per construct) were each inoculated with 25 ml of resuspended culture. BioExpress cell growth media (Cambridge Isotope Laboratories, Inc) was added (2 × 100 ml of 10× U-15N, 98% for the ^{15}N peptide), and cultures were grown at 37 °C with shaking at 250 RPM for 2 to 3 h in the presence of 0.1 mg/ml of kanamycin until an absorbance reading of 0.6 at 600 nm was reached. Peptide expression was induced by adding 10 mg/ml D-lactose, and the cultures were grown for four more hours at 37 °C with shaking at 250 RPM. Cultures were centrifuged, and the peptides were purified by HPLC as described previously.

Expression of PR–R7 Ala constructs

Wildtype PR–R7 with an N-terminal His_6 tag followed by a TEV cleavage site, and an engineered C-terminal Cys residue, cloned into the pET30b(+) vector was used as a starting construct. Residues 22 to 49, constituting the MP region, and the subsequent R7 residues 50 to 69 were converted groupwise (four to five residues, consecutively) to Ala residues through QuikChange site-directed mutagenesis and confirmed by DNA sequencing. The constructs were transformed into *E. coli* Rosetta 2 (DE3), expressed, purified by His_6 tag and TEV cleavage, labeled with 5F, and purified by HPLC as described previously. The peptide concentration was determined from the absorbance at 280 nm using molar extinction coefficients of 10,430 M^{-1} cm^{-1} for PR–R7 constructs with sequences VKYRDA, EYNDG, TFGYE, YKKP, YNVTT, and TATYG changed to Ala residues; and 11,920 M^{-1} cm^{-1} for PR–R7 constructs with sequences GTGIR, ARPT, SETNA, and HADG changed to Alas.

Size-exclusion chromatography and light scattering

Size-exclusion chromatography demonstrated that full-length SC(1–660), but not SC(1–325), interacts with frag D. The size exclusion profile was recorded using a Superdex-200 column (GE, 10 × 300 mm) pre-equilibrated with 50 mM Hepes, 125 mM NaCl, 5 mM $CaCl_2$, and pH 7.4 buffer. In a first set of experiments, 100 µl each of the samples of SC(1–325) (52.67 µM or 2.0 mg/ml); frag D (24.7 µM or 2.1 mg/ml); and 100 µl of a 1:1 mixture of SC(1–325) and frag D in 50 mM Hepes and 125 mM NaCl buffer, pH 7.4, were passed on the column separately. Subsequently, 100 µl each of the samples of SC(1–660) (24.2 µM or 1.8 mg/ml); frag D (24.7 µM/2.1 mg/ml); and 100 µl of a 1:1 mixture of SC(1–660) and frag D in 50 mM Hepes and 125 mM NaCl, pH 7.4, were passed separately on the pre-equilibrated column and eluted using the same buffer as described previously. Elution profiles (absorbance at 280 nm in milliabsorbance *versus* elution volume) were recorded continuously for both sets. Light scattering data were acquired with a PD2010 multidetection light scattering system to obtain the apparent molecular mass (M_r) of the eluted complexes and proteins.

Native PAGE of frag D binding to SC(1–660), [5F]PR–R1, the SC(1–660)·[5F]ProT complex, and labeled C-terminal repeat constructs

SC(1–660) (4 µM) was incubated with 1 to 9× molar excess of frag D for 30 min in 50 mM Hepes, 110 mM NaCl, 5 mM $CaCl_2$, 1 mg/ml PEG-8000 containing 10 µM FFR-CK and FPR-CK at 25 °C, and run on native PAGE along with frag D and SC(1–660) as controls (Fig. 3*C*). The samples were mixed with native sample buffer, 0.32 M Tris, 50% glycerol and 0.1% bromophenol blue, pH 7.6, and electrophoresed at 100 V for 5 to 6 h at 4 °C on a 6% Tris–glycine gel without SDS, using a 0.025 mM Tris, 0.192 mM glycine running buffer, and pH 8.3. Gels were stained for protein with GelCode Blue (Pierce), and fluorescence was visualized with a 300 nm transilluminator.

Mixtures of [5F]PR–R1 (12.2 µM), [5F]R1 (50.0 µM), or [5F]PR (45.0 µM) with ∼0.5-fold to ∼2.0-fold molar excess of frag D were incubated and electrophoresed similarly (Fig. S2).

[5F]ProT (2.5 µM) was incubated with SC(1–660) (3.7 µM) for 30 min, and the complex was reacted with frag D at 7.5, 11.2, 15.0, 18.7, 26.2, and 29.9 µM (Fig. S3). [5F]PR–(R1 → R7) (4.3 µM) was incubated with frag D at 10.0, 15.0, 20.0, 25.0, 30.0, 35.0, and 40.0 µM for 30 min and electrophoresed similarly (Fig. S4).

[5F]PR–R1R6R7 (5.6 µM) and [5F]PR–R1R3R3 (8.1 µM) were incubated with frag D at 5.0, 10.0, 20.0, 30.0, 40.0, 50.0, and 60.0 µM and electrophoresed similarly (Fig. S5).

NMR spectroscopy, data collection, and chemical shift assignments

Titration NMR experiments were performed at 25 °C on a Bruker AV-III 600.13 MHz spectrometer equipped with quadruple resonance cryogenically cooled CPQCI probe. Standard ^{1}H–^{15}N HSQC experiments were used containing a flip-back pulse and Watergate sequence to suppress the water signal (63–65). Titration experiments were done using 200 µl of 65 µM protein solution plus 5 µl D_2O in a 3 mm NMR tube. Various amounts of a 240 µM frag D stock in the same buffer solution were added. All experiments were referenced against the 4,4-dimethyl-4-silapentane-1-sulfonic acid standard, processed with Topspin 3.5 (Bruker BioSpin), and analyzed with NMRView (One Moon Scientific, Inc). Backbone resonance assignments were utilized as described (27).

Fluorescence equilibrium binding of C-terminal repeat peptides to frag D

Fluorescence intensity and anisotropy measurements were performed with a QuantaMaster 30 spectrofluorometer (Photon Technology International). Titrations were performed at 25 °C in 50 mM Hepes, 110 mM NaCl, 5 mM $CaCl_2$ and

1 mg/ml PEG-8000, pH 7.4 buffer with 10 μM FPR-CK inhibitor, at $\lambda_{excitation}$ of 490 nm (1–2 nm band pass) and $\lambda_{emission}$ of 514 nm (1–5 nm band pass) using acrylic cuvettes coated with PEG 20,000. Fluorescein-labeled SC C-terminal repeat constructs, [5F]PR, [5F]R1, [5F]MP, [5F]PR–R1, [5F]PR–R2, [5F]PR–R3, [5F]PR–R6, [5F]PR–R7, and the Ala-mutated constructs [5F]PR–R7-VKYRDA, [5F]PR–R7-GTGIR, [5F]PR–R7-EYNDG, [5F]PR–R7-TFGYE, [5F]PR–R7-ARPT, [5F]PR–R7-YKKP, [5F]PR–R7-SETNA, [5F]PR–R7-YNVTT, [5F]PR–R7-HADG, and [5F]PR–R7-TATYG were titrated with frag D. The fractional change in fluorescence was calculated as $(F_{obs} - F_o)/F_o = \Delta F/F_o$, and the data were fit by the quadratic binding equation (66) (Supporting Information). Nonlinear least-squares fitting was performed with SCIENTIST (MicroMath) to obtain the dissociation constant, K_D, maximum fluorescence intensity $(F_{max} - F_o)/F_o = \Delta F_{max}/F_o$) and stoichiometric factor (n) for the peptide constructs. The error estimates (2SD) represent the 95% confidence interval. Fitting of the Ala constructs was done with the stoichiometric factor (n) fixed to 1, appropriate for titrations with probe concentration below the K_D of the interaction.

To determine whether the repeats bind to the frag D β-holes and γ-holes, [5F]PR–R1 was titrated with frag D in the presence of saturating 4.9 mM GPRP under experimental conditions described previously. The K_D for binding of GPRP to frag D is 20 μM (31). The K_D and maximum fluorescence intensity for frag D binding to [5F]PR–R1 were obtained by fitting the data with n fixed to 1 (Fig. 5).

To determine the effect of pH and NMR buffer conditions, equilibrium binding at pH 7.0 and 7.4 of [5F]PR–R7 (17 and 848 nM, respectively) to frag D was measured in 20 mM sodium phosphate, 150 mM NaCl, and 1 mg/ml PEG-8000 buffers containing 10 μM FPR-CK inhibitor, using $\lambda_{excitation}$ of 490 nm (4 nm band pass at pH 7.0; 2 nm at pH 7.4) and $\lambda_{emission}$ of 514 nm (8 nm band pass at pH 7.0; 4 nm at pH 7.4). The K_D and maximum fluorescence intensity values were obtained as described previously, with n fixed to 1.

Fluorescence anisotropy titrations were performed in the same buffer. Anisotropy measurements were corrected for total intensity changes using a modified Lakowicz equation (67). [5F]PR–(R1 → R7) was titrated with frag D at excitation wavelength $\lambda_{excitation}$ of 495 nm and emission wavelength $\lambda_{emission}$ of 514 nm with band passes ranging from 2 to 6 nm depending on the [5F]PR–(R1 → R7) concentration. Three different [5F]PR–(R1 → R7) preparations were titrated with three different frag D preparations to show reproducibility (Figs. 13 and S8; Table 2). Measurements of r_{obs} as a function of frag D concentration were analyzed by the quadratic binding equation (66) to obtain the dissociation constant K_D and stoichiometric factor n of ligand binding, initial (r_o) and maximal (r_{max}) anisotropies, and the change in anisotropy ($\Delta r = r_{max} - r_o$).

In competitive titrations, mixtures of a fixed concentration of [5F]PR–(R1–R7) with two different concentrations of frag D were each titrated with unlabeled PR–R1R2R3 (three independent batches), PR–R1R6R7, PR–R3R4R7, and PR–R3R6R7 to obtain two data curves for each competitor (Figs. 13 and S8; Table 2). Concentrations of [5F]PR–(R1–R7) and frag D in the competitive titrations are given in the figure legends. Respective sets of direct and competitive titrations were analyzed simultaneously by nonlinear least-squares fitting of the cubic equation in SCIENTIST (MicroMath) (66, 67) (Fig. S11) to obtain the K_D and stoichiometric factor n, initial (r_o) and maximal (r_{max}) anisotropies, and the maximal change in anisotropy ($\Delta r = r_{max} - r_o$) for competitor binding to frag D. Error estimates (±2SD) represent the 95% confidence interval.

Clotting of Fbg by the SC(1–325)·ProT^{QQQ*} and SC(1–660)·ProT^{QQQ*} complexes

Fbg cleavage by T and the SC(1–325)·ProT^{QQQ*} and SC(1–660)·ProT^{QQQ*} complexes was measured as described previously (60). Assays were performed in 50 mM Hepes, 110 mM NaCl, 5 mM $CaCl_2$, 1 mg/ml PEG-8000, and pH 7.4 reaction buffer. Increases in turbidity were measured at 450 nm, 25 °C in a microtiter plate reader, for mixtures of Fbg (0.5 mg/ml) with 10 nM T or 10 nM SC(1–325)·ProT^{QQQ*} complex; and mixtures of Fbg at increasing concentrations (0.3, 0.5, 0.75, and 1.0 mg/ml) with 10 nM SC(1–660)·ProT^{QQQ*} complex. Reactions were started by adding T to the Fbg/buffer mixture or by adding ProT^{QQQ} to the mixtures of Fbg, SC (10 nM), and buffer. Because of the very tight binding of SC(1–325) and SC(1–660) to ProT^{QQQ}, the complex concentrations were estimated to be ∼10 nM. Control reactions were performed without T or ProT^{QQQ}.

CD spectroscopy of SC repeat peptides and frag D

CD spectra of PR–R7 (10.09 μM), PR–(R1 → R7) (3.3 μM), SC(1–325) (2.63 μM), SC(1–660) (1.37 μM), and frag D (3.93 μM) were measured using a Jasco J-810 CD spectrometer from Beckman Coulter, Inc. The spectra were measured in 20 mM sodium phosphate and 150 mM NaCl, pH 7.0 buffer, at peptide/protein concentrations of 0.1 mg/ml. Solutions were inspected for the absence of turbidity. Spectra were measured from 260 to 200 nm with high sensitivity, bandwidth set to 1 nm, response time of 2 s, and scanning speed of 50 nm/min at 25 °C. Each scan represents the average of three individual scans. Data between 190 and 200 nm were noisy, prohibiting accurate analysis in this region. Analysis was performed as described (68) using the formula, [θ] = (100(signal))/cnl, where [θ] is the mean residue ellipticity in deg cm^2 decimol^{-1}, signal is raw output in millidegrees, c is the peptide or protein concentration in millimolar, n is the number of amino acids, and l is the cell path length in centimeter. Ellipticity data were plotted without using a smoothing algorithm (Fig. S9). GOR IV, PSIPRED, and PONDR-FIT secondary structure predictions were performed online as described (40–42).

Data availability

The NMR dataset "PR–R7 from SC of *S. aureus* Newman D2 Tager 104 strain" has been deposited in the Biological Magnetic Resonance Data Bank, with entry ID 27036: https://bmrb.io/data_library/summary/index.php?bmrbId=27036.

All other data are contained within the article and Supporting Information.

Supporting information—This article contains supporting information.

Acknowledgments—The NMR instrumentation used in this work was supported by the National Institutes of Health (NIH) (S10 RR026677) and National Science Foundation (DBI-0922862).

Author contributions—A. A. M., P. P., J. M., P. E. B., and I. M. V. conceptualization; M. V., P. P., J. M., P. E. B., and I. M. V. methodology; A. A. M., M. V., P. P., and J. M. validation; A. A. M., M. V., and I. M. V. formal analysis; A. A. M., M. V., and J. M. investigation; M. V., P. P., J. M., P. E. B., and I. M. V. resources; A. A. M. and I. M. V. data curation; A. A. M. writing–original draft; I. M. V. writing–review & editing; A. A. M. and I. M. V. visualization; P. E. B. and I. M. V. supervision; P. E. B. and I. M. V. project administration; P. E. B. and I. M. V. funding acquisition.

Funding and additional information—This research was supported in part by the NIH R01 HL071544 (to P. E. B. and I. M. V.), R01 HL114477 (to P. P.), and R01 GM080403 (to J. M.). The content is solely the responsibility of the authors and does not necessarily represent the official views of the NIH.

Conflict of interest—The authors declare that they have no conflicts of interest with the contents of this article.

Abbreviations—The abbreviations used are: Ala, alanine; Efb, extracellular Fbg-binding protein; 5F, 5-fluorescein; Fbg, fibrinogen; Fbn, fibrin; FFR-CK, *D*-Phe-Phe-Arg-chloromethyl ketone; FPR-CK, *D*-Phe-Pro-Arg-chloromethyl ketone; frag D, fibrinogen fragment D; GPRP, Gly-Pro-Arg-Pro; HSQC, heteronuclear single quantum coherence; 5-IAF, 5-iodoacetamidofluorescein; me, mol-equivalent; MP, minimal peptide; M_r, relative molecular mass; PR, pseudorepeat; ProT, prothrombin; R1 to R7, repeat 1 to 7; SC, staphylocoagulase; SC(1–660), full-length SC; T, thrombin; TEV, tobacco etch virus.

References

1. Lowy, F. D. (1998) *Staphylococcus aureus* infections. *N. Engl. J. Med.* **339**, 520–532
2. Kourtis, A. P., Hatfield, K., Baggs, J., Mu, Y., See, I., Epson, E., Nadle, J., Kainer, M. A., Dumyati, G., Petit, S., Ray, S. M., Emerging Infections Program MRSA author group, Ham, D., Capers, C., Ewing, H., *et al.* (2019) Vital signs: Epidemiology and recent trends in methicillin-resistant and in methicillin-susceptible *Staphylococcus aureus* Bloodstream infections - United States. *MMWR Morb. Mortal. Wkly. Rep.* **68**, 214–219
3. Watanabe, S., Ito, T., Sasaki, T., Li, S., Uchiyama, I., Kishii, K., Kikuchi, K., Skov, R. L., and Hiramatsu, K. (2009) Genetic diversity of staphylocoagulase genes (coa): Insight into the evolution of variable chromosomal virulence factors in *Staphylococcus aureus*. *PLoS One* **4**, e5714
4. Aung, M. S., Zi, H., Nwe, K. M., Maw, W. W., Aung, M. T., Min, W. W., Nyein, N., Kawaguchiya, M., Urushibara, N., Sumi, A., and Kobayashi, N. (2016) Drug resistance and genetic characteristics of clinical isolates of staphylococci in Myanmar: High prevalence of PVL among methicillin-susceptible *Staphylococcus aureus* belonging to various sequence types. *New Microbes New Infect.* **10**, 58–65
5. Aung, M. S., Urushibara, N., Kawaguchiya, M., Sumi, A., Takahashi, S., Ike, M., Ito, M., Habadera, S., and Kobayashi, N. (2019) Molecular epidemiological characterization of *Staphylococcus argenteus* clinical isolates in Japan: Identification of three Clones (ST1223, ST2198, and ST2550) and a novel staphylocoagulase Genotype XV. *Microorganisms* **7**, 389
6. Vandenesch, F., Lebeau, C., Bes, M., McDevitt, D., Greenland, T., Novick, R. P., and Etienne, J. (1994) Coagulase deficiency in clinical isolates of *Staphylococcus aureus* involves both transcriptional and post-transcriptional defects. *J. Med. Microbiol.* **40**, 344–349
7. Cheng, A. G., Kim, H. K., Burts, M. L., Krausz, T., Schneewind, O., and Missiakas, D. M. (2009) Genetic requirements for *Staphylococcus aureus* abscess formation and persistence in host tissues. *FASEB J.* **23**, 3393–3404
8. Kobayashi, S. D., Malachowa, N., and DeLeo, F. R. (2015) Pathogenesis of *Staphylococcus aureus* abscesses. *Am. J. Pathol.* **185**, 1518–1527
9. Miajlovic, H., Loughman, A., Brennan, M., Cox, D., and Foster, T. J. (2007) Both complement- and fibrinogen-dependent mechanisms contribute to platelet aggregation mediated by *Staphylococcus aureus* clumping factor B. *Infect. Immun.* **75**, 3335–3343
10. Josefsson, E., Higgins, J., Foster, T. J., and Tarkowski, A. (2008) Fibrinogen binding sites P336 and Y338 of clumping factor A are crucial for *Staphylococcus aureus* virulence. *PLoS One* **3**, e2206
11. McNamara, C., Zinkernagel, A. S., Macheboeuf, P., Cunningham, M. W., Nizet, V., and Ghosh, P. (2008) Coiled-coil irregularities and instabilities in group A *Streptococcus* M1 are required for virulence. *Science* **319**, 1405–1408
12. Flick, M. J., Du, X., Prasad, J. M., Raghu, H., Palumbo, J. S., Smeds, E., Höök, M., and Degen, J. L. (2013) Genetic elimination of the binding motif on fibrinogen for the S. aureus virulence factor ClfA improves host survival in septicemia. *Blood* **121**, 1783–1794
13. Ko, Y. P., Kuipers, A., Freitag, C. M., Jongerius, I., Medina, E., van Rooijen, W. J., Spaan, A. N., van Kessel, K. P., Höök, M., and Rooijakkers, S. H. (2013) Phagocytosis escape by a *Staphylococcus aureus* protein that connects complement and coagulation proteins at the bacterial surface. *PLoS Pathog.* **9**, e1003816
14. Herrmann, M., Lai, Q. J., Albrecht, R. M., Mosher, D. F., and Proctor, R. A. (1993) Adhesion of *Staphylococcus aureus* to surface-bound platelets: Role of fibrinogen/fibrin and platelet integrins. *J. Infect. Dis.* **167**, 312–322
15. Panizzi, P., Nahrendorf, M., Figueiredo, J. L., Panizzi, J., Marinelli, B., Iwamoto, Y., Keliher, E., Maddur, A. A., Waterman, P., Kroh, H. K., Leuschner, F., Aikawa, E., Swirski, F. K., Pittet, M. J., Hackeng, T. M., *et al.* (2011) *In vivo* detection of *Staphylococcus aureus* endocarditis by targeting pathogen-specific prothrombin activation. *Nat. Med.* **17**, 1142–1146
16. Maddur, A. A., Panizzi, P., Fuentes-Prior, P., and Bock, P. E. (2011) Interaction of fibrinogen with the staphylocoagulase•prothrombin* complex. *FASEB Proteases in Hemostasis & Vascular Biology Conference*, Carefree, AZ, June 12–17, 2011. Abstract #27.
17. Huber, R., and Bode, W. (1978) Structural basis of activation and action of trypsin. *Acc. Chem. Res.* **11**, 114–122
18. Khan, A., and James, M. (1998) Molecular mechanisms for the conversion of zymogens ro active proteolytic enzymes. *Protein Sci.* **7**, 815–836
19. Friedrich, R., Panizzi, P., Fuentes-Prior, P., Richter, K., Verhamme, I., Anderson, P. J., Kawabata, S., Huber, R., Bode, W., and Bock, P. E. (2003) Staphylocoagulase is a prototype for the mechanism of cofactor-induced zymogen activation. *Nature* **425**, 535–539
20. Maddur, A. A., Kroh, H. K., Aschenbrenner, M. E., Gibson, B. H. Y., Panizzi, P., Sheehan, J. H., Meiler, J., Bock, P. E., and Verhamme, I. M. (2020) Specificity and affinity of the N-terminal residues in staphylocoagulase in binding to prothrombin. *J. Biol. Chem.* **295**, 5614–5625
21. Panizzi, P., Friedrich, R., Fuentes-Prior, P., Richter, K., Bock, P. E., and Bode, W. (2006) Fibrinogen substrate recognition by staphylocoagulase. (pro)thrombin complexes. *J. Biol. Chem.* **281**, 1179–1187
22. Phonimdaeng, P., O'Reilly, M., Nowlan, P., Bramley, A. J., and Foster, T. J. (1990) The coagulase of *Staphylococcus aureus* 8325-4. Sequence analysis and virulence of site-specific coagulase-deficient mutants. *Mol. Microbiol.* **4**, 393–404
23. Schwarzkopf, A., and Karch, H. (1994) Genetic variation in *Staphylococcus aureus* coagulase genes: Potential and limits for use as epidemiological marker. *J. Clin. Microbiol.* **32**, 2407–2412
24. Heilmann, C., Herrmann, M., Kehrel, B. E., and Peters, G. (2002) Platelet-binding domains in 2 fibrinogen-binding proteins of *Staphylococcus aureus* identified by phage display. *J. Infect. Dis.* **186**, 32–39

25. McDevitt, D., Vaudaux, P., and Foster, T. J. (1992) Genetic evidence that bound coagulase of *Staphylococcus aureus* is not clumping factor. *Infect. Immun.* **60**, 1514–1523
26. Maddur, A. A., Voehler, M., Panizzi, P. R., Sheehan, J., Verhamme, I. M., Meiler, J., and Bock, P. E. (2017) Dual mode of interaction of fibrinogen with the Staphylocoagulase•Prothrombin* complex. *Research and Practice in Thrombosis and Haemostasis RPTH, Abstracts XXVI ISTH Congress*, Berlin July 8–13, 2017 1, 386.
27. Voehler, M., Ashoka, M. A., Meiler, J., and Bock, P. E. (2017) Carbon and amide detect backbone assignment methods of a novel repeat protein from the staphylocoagulase in *S. aureus*. *Biomol. NMR Assign.* **11**, 243–249
28. Ko, Y. P., Kang, M., Ganesh, V. K., Ravirajan, D., Li, B., and Höök, M. (2016) Coagulase and efb of *Staphylococcus aureus* have a common fibrinogen binding motif. *mBio* **7**. e01885-15
29. Thomas, S., Liu, W., Arora, S., Ganesh, V., Ko, Y. P., and Höök, M. (2019) The complex fibrinogen interactions of the *Staphylococcus aureus* coagulases. *Front. Cell Infect. Microbiol.* **9**, 106
30. Panizzi, P., Friedrich, R., Fuentes-Prior, P., Kroh, H. K., Briggs, J., Tans, G., Bode, W., and Bock, P. E. (2006) Novel fluorescent prothrombin analogs as probes of staphylocoagulase-prothrombin interactions. *J. Biol. Chem.* **281**, 1169–1178
31. Laudano, A. P., and Doolittle, R. F. (1978) Synthetic peptide derivatives that bind to fibrinogen and prevent the polymerization of fibrin monomers. *Proc. Natl. Acad. Sci. U. S. A.* **75**, 3085–3089
32. Spraggon, G., Everse, S. J., and Doolittle, R. F. (1997) Crystal structures of fragment D from human fibrinogen and its crosslinked counterpart from fibrin. *Nature* **389**, 455–462
33. Everse, S. J., Spraggon, G., Veerapandian, L., and Doolittle, R. F. (1999) Conformational changes in fragments D and double-D from human fibrin(ogen) upon binding the peptide ligand Gly-His-Arg-Pro-amide. *Biochemistry* **38**, 2941–2946
34. Shen, Y., Delaglio, F., Cornilescu, G., and Bax, A. (2009) TALOS plus: A hybrid method for predicting protein backbone torsion angles from NMR chemical shifts. *J. Biomol. NMR* **44**, 213–223
35. Donnini, S., Tegeler, F., Groenhof, G., and Grubmuller, H. (2011) Constant pH molecular dynamics in explicit solvent with lambda-dynamics. *J. Chem. Theor. Comput.* **7**, 1962–1978
36. Kamath, P., and Krishnaswamy, S. (2008) Fate of membrane-bound reactants and products during the activation of human prothrombin by prothrombinase. *J. Biol. Chem.* **283**, 30164–30173
37. Woody, R. W. (1994) Contributions of tryptophan side chains to the far-ultraviolet circular dichroism of proteins. *Eur. Biophys. J.* **23**, 253–262
38. Lau, S. Y., Taneja, A. K., and Hodges, R. S. (1984) Synthesis of a model protein of defined secondary and quaternary structure. Effect of chain length on the stabilization and formation of two-stranded alpha-helical coiled-coils. *J. Biol. Chem.* **259**, 13253–13261
39. Zhou, N. E., Kay, C. M., and Hodges, R. S. (1992) Synthetic model proteins. Positional effects of interchain hydrophobic interactions on stability of two-stranded alpha-helical coiled-coils. *J. Biol. Chem.* **267**, 2664–2670
40. Garnier, J., Gibrat, J. F., and Robson, B. (1996) GOR method for predicting protein secondary structure from amino acid sequence. *Methods Enzymol.* **266**, 540–553
41. Jones, D. T. (1999) Protein secondary structure prediction based on position-specific scoring matrices. *J. Mol. Biol.* **292**, 195–202
42. Xue, B., Dunbrack, R. L., Williams, R. W., Dunker, A. K., and Uversky, V. N. (2010) PONDR-FIT: A meta-predictor of intrinsically disordered amino acids. *Biochim. Biophys. Acta* **1804**, 996–1010
43. McGavin, M. H., Krajewska-Pietrasik, D., Ryden, C., and Höök, M. (1993) Identification of a *Staphylococcus aureus* extracellular matrix-binding protein with broad specificity. *Infect. Immun.* **61**, 2479–2485
44. Boden, M. K., and Flock, J. I. (1994) Cloning and characterization of a gene for a 19 kDa fibrinogen-binding protein from *Staphylococcus aureus*. *Mol. Microbiol.* **12**, 599–606
45. McDevitt, D., Francois, P., Vaudaux, P., and Foster, T. J. (1994) Molecular characterization of the clumping factor (fibrinogen receptor) of *Staphylococcus aureus*. *Mol. Microbiol.* **11**, 237–248
46. Ni Eidhin, D., Perkins, S., Francois, P., Vaudaux, P., Höök, M., and Foster, T. J. (1998) Clumping factor B (ClfB), a new surface-located fibrinogen-binding adhesin of *Staphylococcus aureus*. *Mol. Microbiol.* **30**, 245–257
47. Palma, M., Haggar, A., and Flock, J. I. (1999) Adherence of *Staphylococcus aureus* is enhanced by an endogenous secreted protein with broad binding activity. *J. Bacteriol.* **181**, 2840–2845
48. Wann, E. R., Gurusiddappa, S., and Höök, M. (2000) The fibronectin-binding MSCRAMM FnbpA of *Staphylococcus aureus* is a bifunctional protein that also binds to fibrinogen. *J. Biol. Chem.* **275**, 13863–13871
49. Boden, M. K., and Flock, J. I. (1992) Evidence for three different fibrinogen-binding proteins with unique properties from *Staphylococcus aureus* strain Newman. *Microb. Pathog.* **12**, 289–298
50. Watanabe, S., Ito, T., Takeuchi, F., Endo, M., Okuno, E., and Hiramatsu, K. (2005) Structural comparison of ten serotypes of staphylocoagulases in *Staphylococcus aureus*. *J. Bacteriol.* **187**, 3698–3707
51. Negron, O., and Flick, M. J. (2019) Does fibrinogen serve the host or the microbe in Staphylococcus infection? *Curr. Opin. Hematol.* **26**, 343–348
52. Retzinger, G. S., Cook, B. C., and Deanglis, A. P. (1994) The binding of fibrinogen to surfaces and the identification of 2 distinct surface-bound species of the protein. *J. Colloid Interf. Sci.* **168**, 514–521
53. Cheng, A. G., McAdow, M., Kim, H. K., Bae, T., Missiakas, D. M., and Schneewind, O. (2010) Contribution of coagulases towards *Staphylococcus aureus* disease and protective immunity. *PLoS Pathog.* **6**, e1001036
54. Dunker, A. K., Cortese, M. S., Romero, P., Iakoucheva, L. M., and Uversky, V. N. (2005) Flexible nets. The roles of intrinsic disorder in protein interaction networks. *FEBS J.* **272**, 5129–5148
55. Uversky, V. N. (2019) Intrinsically disordered proteins and their "mysterious" (meta)physics. *Front. Phys.* **7**, 1–18
56. Everse, S. J., Pelletier, H., and Doolittle, R. F. (1995) Crystallization of fragment D from human fibrinogen. *Protein Sci.* **4**, 1013–1016
57. Marder, V. J., Budzynski, A. Z., and James, H. L. (1972) High molecular weight derivatives of human fibrinogen produced by plasmin. 3. Their NH2-terminal amino acids and comparison with the "NH2-terminal disulfide knot". *J. Biol. Chem.* **247**, 4775–4781
58. Friedrich, R., Panizzi, P., Kawabata, S., Bode, W., Bock, P. E., and Fuentes-Prior, P. (2006) Structural basis for reduced staphylocoagulase-mediated bovine prothrombin activation. *J. Biol. Chem.* **281**, 1188–1195
59. Panizzi, P., Boxrud, P. D., Verhamme, I. M., and Bock, P. E. (2006) Binding of the COOH-terminal lysine residue of streptokinase to plasmin(ogen) kringles enhances formation of the streptokinase.plasmin(ogen) catalytic complexes. *J. Biol. Chem.* **281**, 26774–26778
60. Kroh, H. K., Panizzi, P., and Bock, P. E. (2009) Von Willebrand factor-binding protein is a hysteretic conformational activator of prothrombin. *Proc. Natl. Acad. Sci. U. S. A.* **106**, 7786–7791
61. Anthis, N. J., and Clore, G. M. (2013) Sequence-specific determination of protein and peptide concentrations by absorbance at 205 nm. *Protein Sci.* **22**, 851–858
62. Bock, P. E. (1992) Active-site-selective labeling of blood coagulation proteinases with fluorescence probes by the use of thioester peptide chloromethyl ketones. I. Specificity of thrombin labeling. *J. Biol. Chem.* **267**, 14963–14973
63. Grzesiek, S., and Bax, A. (1993) The importance of not saturating H_2O in protein NMR - Application to sensitivity enhancement and NOE measurements. *J. Am. Chem. Soc.* **115**, 12593–12594
64. Kay, L. E., Keifer, P., and Saarinen, T. (1992) Pure absorption gradient enhanced heteronuclear single quantum correlation spectroscopy with improved sensitivity. *J. Am. Chem. Soc.* **114**, 10663–10665
65. Palmer, A. G., Cavanagh, J., Wright, P. E., and Rance, M. (1991) Sensitivity improvement in proton-detected 2-dimensional heteronuclear correlation NMR-spectroscopy. *J. Magn. Reson.* **93**, 151–170
66. Bock, P. E., Olson, S. T., and Björk, I. (1997) Inactivation of thrombin by antithrombin is accompanied by inactivation of regulatory exosite I. *J. Biol. Chem.* **272**, 19837–19845
67. Newell-Caito, J. L., Laha, M., Tharp, A. C., Creamer, J. I., Xu, H., Maddur, A. A., Tans, G., and Bock, P. E. (2011) Notecarin D binds human factor V and factor Va with high affinity in the absence of membranes. *J. Biol. Chem.* **286**, 38286–38297
68. Myers, J. K., Pace, C. N., and Scholtz, J. M. (1997) Helix propensities are identical in proteins and peptides. *Biochemistry* **36**, 10923–10929